Chapter 1

The Case for Optical/Infrared Space Interferometry

Jonah T Hansen, 2023

1.1 The Current Field of Exoplanet Research

1.1.1 The Quest for Biosignatures

If you could go back in time and ask an astronomer in the early 1990s what the biggest sub-discipline in astronomy would be in 30 years, I'm certain that almost none of them would have mentioned the field of exoplanets. In fact, the first exoplanet orbiting a main sequence star, 51 Peg b, was only discovered in 1995 by Mayor & Queloz [1995]. However, fast forward to today and the field of exoplanets, that is, the study of planets that orbit around stars other than the sun, is arguably the fastest-growing discipline within astronomy. Currently, according to the NASA Exoplanet Archive [NASA Exoplanet Science Institute, 2023], we have detected over 5000 confirmed exoplanets - a huge number considering we knew about less than 1000 ten years ago and none 30 years ago.

One just has to look at the recent Astro2020 decadal survey [National Academies of Sciences, Engineering, and Medicine, 2021] produced by the astronomical community in the United States to see the major emphasis on exoplanets. "Worlds and Suns in context" is one of the three major science themes that frames the decadal survey's scientific vision, and one of the three flagship programs is "Pathways to Habitable Worlds", a program that aims to "identify and characterise Earth-like extrasolar planets, with the ultimate goal of obtaining imaging and spectroscopy of potentially habitable worlds". It is this last sentence that likely explains why the sub-discipline of exoplanets generates such fervent interest. Within it, we can begin to tackle one of the most profound questions our human species can ask: "are we alone in the universe?"

We can see the interest in this question far outside the confines of the astronomical research community; from science fiction novels and movies sparking our imaginations as to what aliens might be like, to philosophical and theological discussions on what it means for us as a species to be alive. The question also branches into environmentalism: if our planet is the only habitable planet out there, surely we should do our very best to protect this precious resource. The profound implications of "are we alone?", entices even the most sceptical researcher to attempt to answer it.

Out of all exoplanets though, some present as much more interesting than others; the most tantalising of which are Earth-like exoplanets around solar-type stars. This was the primary mission of the *Kepler* space mission [Borucki et al., 2010]: to determine how many Earth-sized (that is, rocky) exoplanets lie inside the habitable zone of solar-type stars (primarily of types F, G and K), a parameter known as "η_E" [Bryson et al., 2021]. Here, habitable zone (HZ) has many definitions in the literature (see Kasting et al. [1993]; Kopparapu et al. [2013] and the references therin), ranging from human habitability [e.g. Dole, 1964] to the presence of liquid water [e.g. Kasting et al., 1993] among others [e.g. McIntyre et al., 2023]. This is generally parameterised as a function of stellar insolation, with cooler stars having close-in HZs [e.g. Huang, 1959; Kasting et al., 1993; Kopparapu et al., 2013]. The reason that terrestrial planets around the HZ of solar-type stars are so critical to study, is that these are the best targets for life as we know it here on Earth. So far we only know life exists on Earth, so it makes sense for missions looking for life elsewhere to prioritise looking for "exoEarths" [Stark et al., 2014].

As professional astronomers, how do we attempt to answer this question? We must rely on a concept known as "biosignatures". According to Schwieterman et al. [2018], these are "the presence of a gas or other feature that may be indicative of a biological agent". An alternative definition by Léger et al. [2011] is "an observable feature of a planet, such as its atmospheric composition, that our present models cannot reproduce when including the abiotic physical and chemical processes we know about". These biosignatures may come in the form of direct morphological evidence of ancient lifeforms, such as those proposed for Mars [e.g. McKay et al., 1996] (albeit heavily debated, see Steele et al. [2006]), or measurements of surface chemistry such as that on Titan [e.g. Barnes et al., 2021]. Signals may also come in the form of technosignatures: "signals of engineering/technology that are distinguishable from astrophysical processes" [Price et al., 2020]. However, unlike with planetary science, we are unable to send probes such as the 2020 Mars rover *Perserverance* [Vago et al., 2017], or the proposed *Europa Lander* [Hand et al., 2022] to directly look for signs of life on exoplanets. Instead we must rely on the analysis of spectral or polarisation features emerging from the detected radiation from an exoplanet's atmosphere [Des Marais et al., 2002].

We already have a proof of concept of this idea, notably in the study of Sagan et al. [1993]. In this seminal work, the authors used the *Galileo* spacecraft as it flew past Earth in 1990 to obtain a spectrum of the Earth's atmosphere, finding that a number of molecules, including oxygen and atmospheric methane, were out of thermodynamic equilibrium. This, combined with a sharp absorption feature in the red end of the visible spectrum (due to photosynthetic life, see Seager et al. [2005]), were enough to conclude *a priori* that life existed on Earth. While what exactly makes up a biosignature is still a matter of debate [e.g. Arnold et al., 2002; Léger et al., 2011; Schwieterman et al., 2018], taking this technique and extending it to truly unknown systems (ideally exoEarths) is the goal of many exoplanet astronomers [e.g. Des Marais et al., 2002; Schwieterman et al., 2018; Quanz et al., 2022].

1.1.2 Current Detection Methods

The quest for biosignatures is not an easy task though, as most current exoplanet detection methods do not allow such an analysis. In Figure 1.1, the approximately 5000 confirmed exoplanets currently in NASA's exoplanet archive [NASA Exoplanet Science Institute, 2023] are plotted as a function of mass, period and detection technique. Overplotted is the position of Earth, and noticeably the parameter space surrounding Earth contains a dearth of planets. The current detection techniques are also summarised in Table 1.1, with many of them being incapable of detecting biosignatures and informing whether the planet is habitable.

The first technique used to discover a planet around a main sequence star

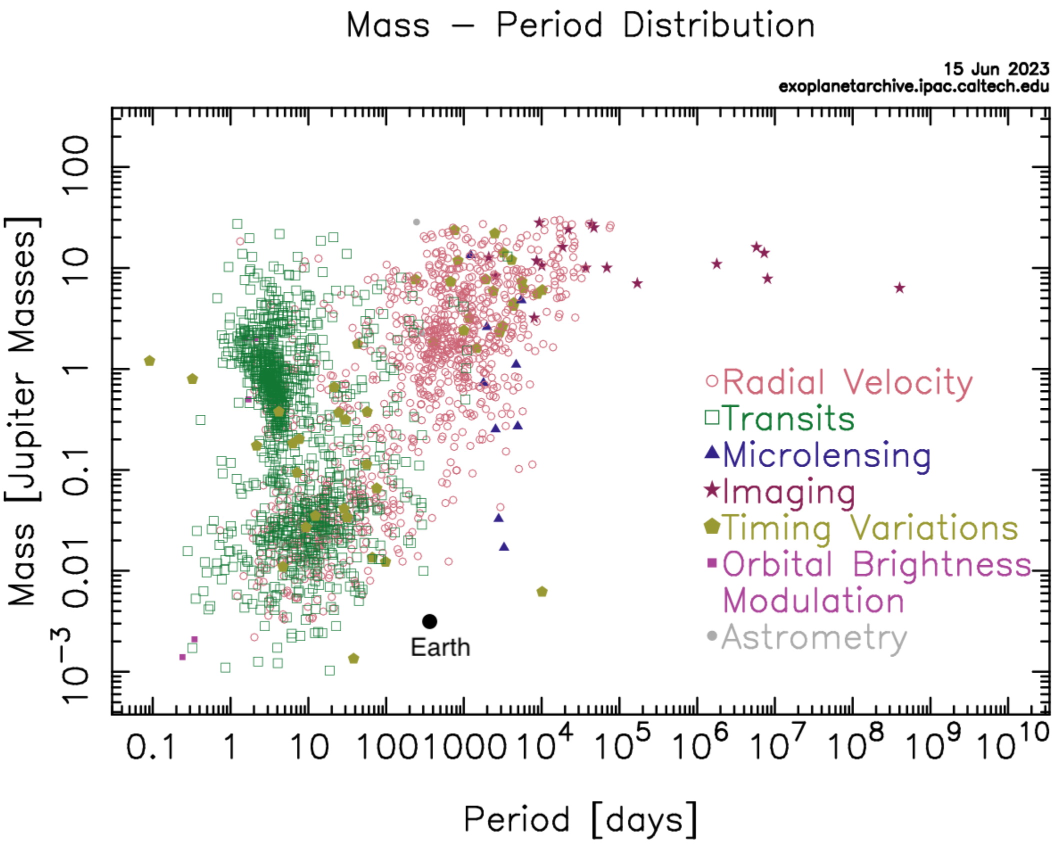

Figure 1.1: Mass/period distribution of the approximately 5000 currently confirmed exoplanets listed in the NASA Exoplanet Archive [NASA Exoplanet Science Institute, 2023]. Planets are coloured by detection method. Note that only planets with known radius and mass information are plotted. The location of Earth is also included for comparison.

Table 1.1: Exoplanet detection techniques, showing the current number of detections and year of first detection. Note that the first exoplanet transit was detected for a known planet and was detected by two different groups simultaneously.

Detection Method	Number Detected	First Year of Detection	Reference
Radial Velocity	1048	1995	Mayor & Queloz [1995]
Transits	4092	1999 (First transit); 2002 (First detection)	Henry et al. [2000], Charbonneau et al. [2000]; Konacki et al. [2003]
Microlensing	200	2003	Bond et al. [2004]
Imaging	67	2004	Chauvin et al. [2004]
Timing Variations	51	1992 (Pulsar); 2011 (TTV)	Wolszczan & Frail [1992]; Ballard et al. [2011]
Astrometry	1	2022	Curiel et al. [2022]
Others	10	-	-

is known as the radial velocity technique. Due to planetary bodies exerting gravity on their host star, the stellar host will undergo reflex motion in proportion to the mass ratio. While this is extremely hard to see with proper motions (see the discussion on astrometry later), one can use Doppler spectroscopy to see the star's motion along the radial velocity axis. The first successful use of this technique was by Mayor & Queloz [1995], who found a planet of approximately Jupiter mass orbiting around the star 51 Peg. A plot of the radial velocity over the course of an orbit is shown in Figure 1.2.

If the radial velocity can be measured at all phases of an orbit, then a number of orbital parameters can be extracted: the period T, the eccentricity e, the argument of periapse ω, the time of periapse passage T_0 and the semi-major amplitude of the radial velocity K_1. Using Kepler's third law, the period can then be used to obtain the semi-major axis a of the orbit, and then from Lovis & Fischer [2010], we can obtain an estimate of the mass through the relation:

$$K_1 = \frac{28.4329 \text{ ms}^{-1}}{\sqrt{1-e^2}} \frac{m_2 \sin i}{\mathrm{M_J}} \left(\frac{m_1 + m_2}{\mathrm{M}_\odot}\right)^{-\frac{2}{3}} \left(\frac{a}{1 \text{ AU}}\right)^{-\frac{1}{2}}, \tag{1.1}$$

where m_2 is the mass of the planet in terms of Jupiter's mass, and m_1 is the mass of the star in solar masses.

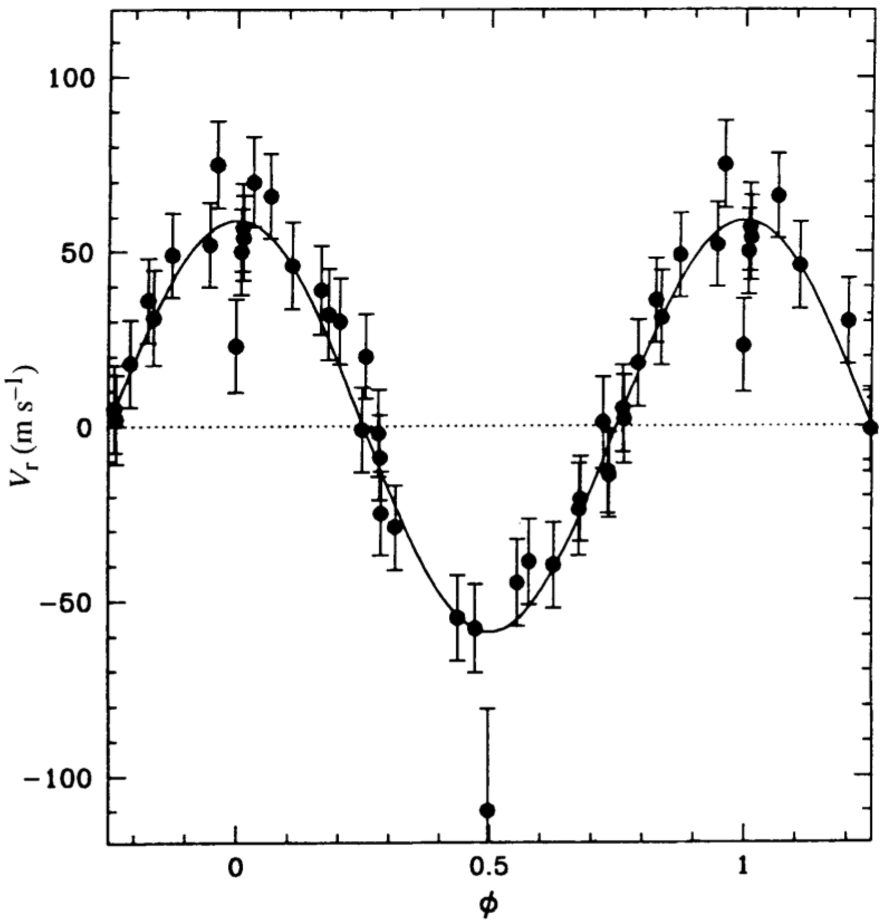

Figure 1.2: Radial velocity curve of the star 51 Peg, taken from Mayor & Queloz [1995].

That being said, only the minimum mass can be identified due to the unknown inclination i of the orbit. Secondly, because we are only measuring the orbital dynamics of the star-planet pair, we do not obtain any spectral information about the planet and hence cannot say anything about the presence of biosignatures in the atmosphere. Nevertheless, it is still one of the most successful planet detection techniques. Furthermore it is very useful in estimating the mass of the planet, which when combined with radius information can be used to determine the planet's density and composition; informing some questions about potential habitability.

The transit detection method is arguably the most successful technique in discovering exoplanets, owing largely to the over 2,300 confirmed exoplanets [Bryson et al., 2021] detected by the *Kepler* telescope [Borucki et al., 2010]. The method is rather straightforward: if a planet around a star has an orbital inclination of approximately zero, and if we then observe that star for a long enough period, then we should be able to see the planet pass in between our line of sight to the star, dimming the flux. As planet orbits are periodic, this means that such an event should happen periodically, allowing us to confirm the transit event as being caused by a planet. A series of light curves (that is, the flux of the star as a function of time) of the star WASP-72 is shown in Figure 1.3 [Wong et al., 2020].

As this is not a dynamical technique, we are not able to estimate the mass of the planetary companion. However, and very importantly, we can extract the star-to-planet radius ratio $R_P/R_\star$ through the transit depth measured as a fractional decrease in flux δ: $R_P/R_\star = \sqrt{\delta}$. Because we only extract the radius ratio, this does mean that we need to have a precise measurement of the stellar radius to find the planetary radius. Two such methods of calibrating the radius include optical inteferometry [e.g. Brown, 1968; Boyajian et al., 2012; Rains et al., 2020], or spectral fitting to cool stars using binary pairs [e.g. Rains et al., 2021]. Having the radius, one can then take follow-up radial velocity measurements to thus obtain most of the parameters of an exoplanet including the stellar mean density and the planet's surface gravity [Winn, 2010], with the exception of spectral data needed to inform the presence of biosignatures.

Spectral information can be obtained, however, through the relatively new technique of transmission spectroscopy; analysing the spectrum of a stellar

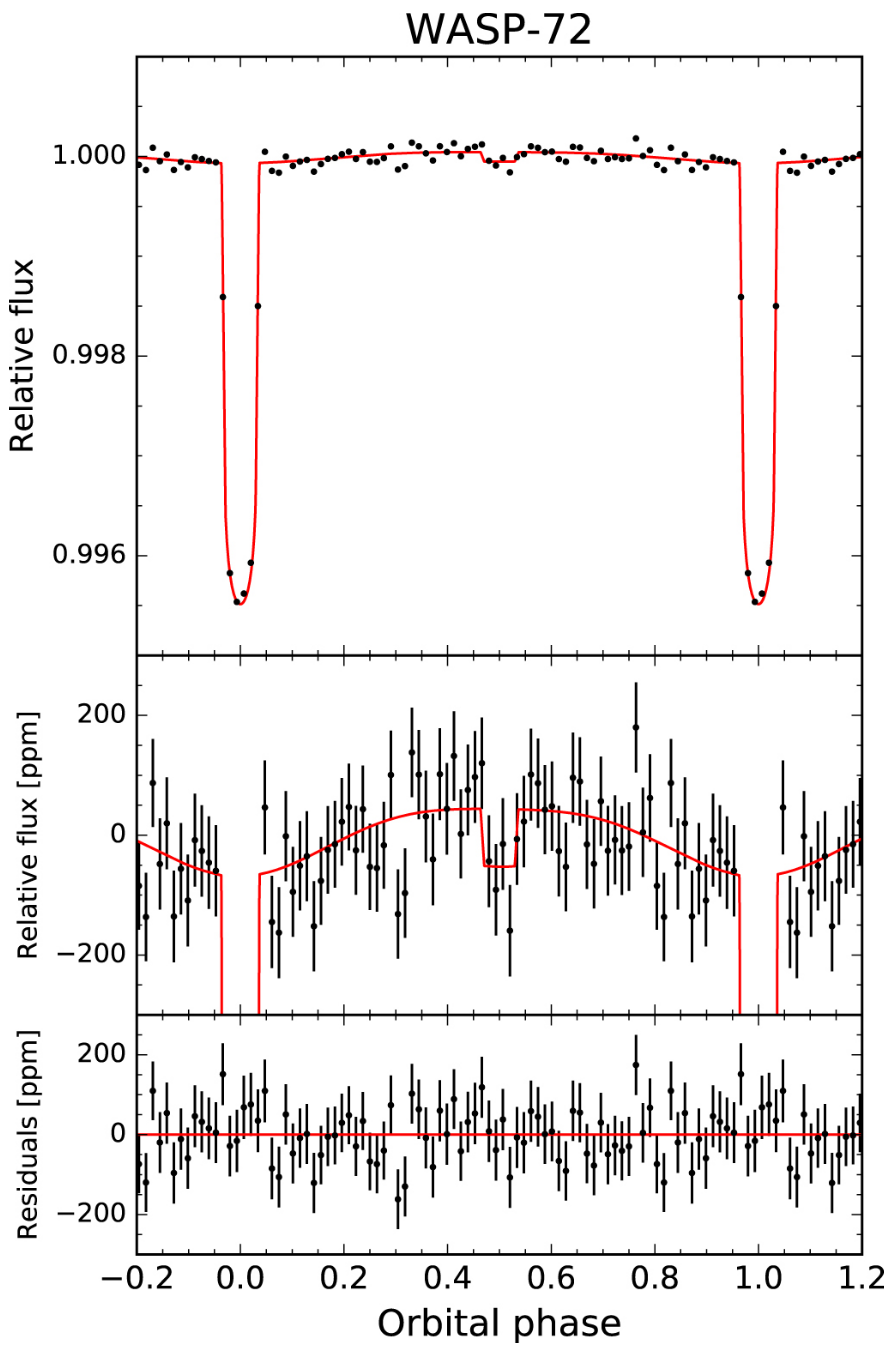

Figure 1.3: Transit light curves of the star WASP-72, taken from Wong et al. [2020]

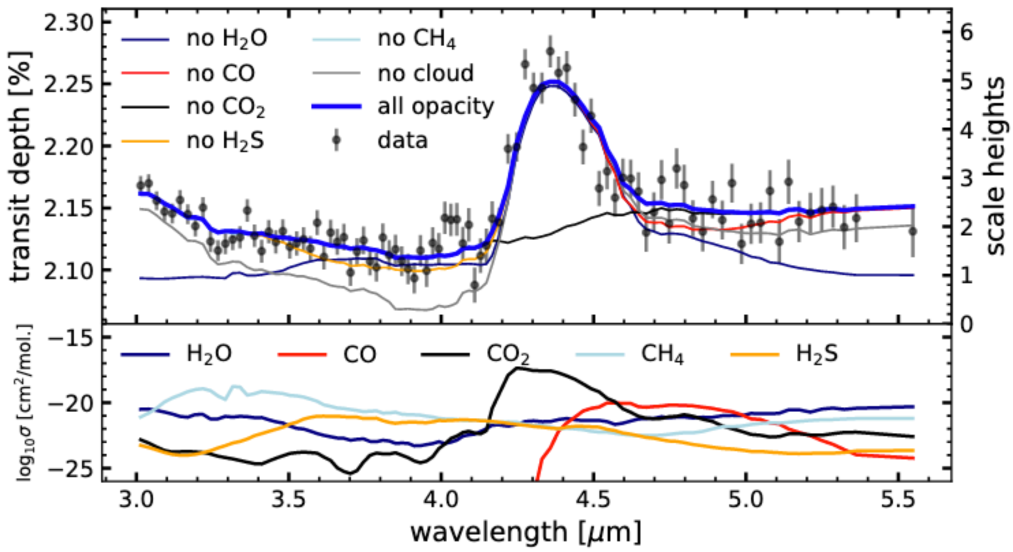

Figure 1.4: Transmission spectrum of WASP-39b, taken from JWST Transiting Exoplanet Community Early Release Science Team et al. [2023]

host as its planetary companion goes in and out of transit and indirectly retrieving the planetary spectrum. This comes in two flavours: primary transit and secondary eclipse spectroscopy [Tinetti & Beaulieu, 2009]. The former is achieved by noting that, while a planet with an atmosphere is transiting in front of the star, a fraction of the light from the star will be scattered and absorbed by the thin atmosphere. This will vary by wavelength and increase the transit depth by a small amount $\Delta\delta$; a proxy for the atmospheric spectrum [Winn, 2010]. One such atmospheric retrieval of the planet WASP-39 b, captured with the James Webb Space Telescope's (JWST) NIRSpec, is shown in Figure 1.4 [JWST Transiting Exoplanet Community Early Release Science Team et al., 2023]; in the plot, we can see that CO_2 absorption was detected. Unfortunately though, the transmission spectroscopy signal is strongly biased towards large planets and atmospheres with sizeable scale heights, or small stars (i.e. not terrestrial planets around solar stars) and the signals for Earth-like transits are smaller than the granulation noise from stellar surface inhomogeneities [e.g. Rackham et al., 2018; Barclay et al., 2021].

The second technique uses the secondary eclipse: where the planet goes behind the star, causing the light curve to produce a small dip in-between primary transits (also seen in Figure 1.3). This decrease in light is due to the blocking of scattered visible light, or emitted thermal radiation of the planet; hence if the spectrum of the star during the eclipse is subtracted from the spectrum before the eclipse, what remains should be the scattered/emitted spectrum of the planet [Tinetti & Beaulieu, 2009]. However, this also has inherent problems with the size of the signal; usually even smaller than the primary transit method [Winn, 2010] and hence very prone to uncertainties in the stellar spectrum.

Both of these techniques, while consistently improving, are not feasible for the study of terrestrial exoplanetary biosignatures. To emphasise this point, consider a nearby Earth-like planet around a solar-type star at 50 pc (chosen due to transit probability). If we assume a 17 km atmospheric cross section, from twice the 8.5 km scale height of Earth's N_2 rich atmosphere [Ahrens, 1995], we obtain a transit depth of 4.5 $\times 10^{-7}$. This requires on the order of 10^{14} photons to achieve a five sigma detection of an atmospheric absorption feature. In the near infrared L (3.5 μm) band at 50 pc, a solar-type star would emit on the order of 10^6 photons/s/m^2. Hence, for JWST operating at 50% efficiency, one would require a minimum of 75 days of integration or equivalently a staggering 300 years worth of transits. Increasing the amount of collected photons by an order of magnitude (such as a brighter star or using a bigger telescope) still does not make detecting terrestrial biosignatures in this way realistic. Hence, transit spectroscopy is only useful for either planets with hydrogen-rich atmospheres (i.e. large atmospheric scale heights) or for planets around much smaller stars such as M dwarfs.

Another technique that has been successful in detecting planets is that of microlensing: when a star passes directly in front of a background star, its gravitational field will effectively create a lens, bending and amplifying the light of the background star into an "Einstein ring" [Gaudi, 2012]. This effectively creates a spike in the light curve of the background star. Now, if the foreground star has a planetary companion, the planet's gravitational field will superimpose another, smaller peak on the light curve. From the shape of the microlensed light curve, the mass ratio of the star/planet system and some of its orbital properties can be calculated [Gaudi, 2010] but notably, no spectral information can be inferred. Furthermore, microlensing events are spontaneous and are often of short duration, and as the light from the planet and host star are usually faint, microlensed planets are extremely difficult to follow up with other techniques [Gaudi, 2012].

Skipping over direct imaging (which we will discuss in the next section), we come to a collection of techniques that concern timing variations. This includes pulsar timing, used to discover the very first exoplanet [Wolszczan & Frail, 1992]. This method works similarly to the radial velocity method, except the planet is perturbing the precise pulsation of a host pulsar rather than it's radial velocity. The extreme precision of pulsar pulses means that this method is sensitive to large asteroid sized masses, but due to the rarity of pulsars it is not used frequently [Wolszczan & Kuchner, 2010]. Another technique is transit timing variation (TTV), where a second planet perturbs the periodic transit signal from another transiting planet and was first successfully used by Ballard et al. [2011]. However, this suffers from the same inclination bias as the transit technique due to its reliance on transits. Other timing techniques include perturbations to the pulsation periodicity of variable stars [e.g. Silvotti et al., 2007], and perturbations to the eclipse period of binary stars [e.g. Qian et al., 2010]. None of these provide spectral information needed for biosignature detection.

Finally, I briefly mention the astrometry method here despite the detection of very few planets [e.g. Curiel et al., 2022]. This method is akin to radial velocity, but looks instead for the perturbations of the proper motion of the star in the plane of the sky. The complementarity of astrometry to other detection methods is that it breaks the inclination ambiguity and can thus provide the true mass of the planet (not just a lower limit), and is also more sensitive to planets with longer periods (whereas the radial velocity method is more sensitive to shorter period planets). This astrometric signal, as given by Quirrenbach [2010], is:

$$\theta = 3\ \mu\text{as} \left(\frac{m_p}{\mathrm{M_E}}\right) \left(\frac{m_\star}{\mathrm{M_\odot}}\right)^{-\frac{2}{3}} \left(\frac{P}{\mathrm{yr}}\right)^{\frac{2}{3}} \left(\frac{d}{\mathrm{pc}}\right)^{-1}, \tag{1.2}$$

where m_p is the planet mass in Earth masses, $m_\star$ is the stellar mass in solar masses, P is the period in years and d is the distance in parsecs.

This signal is extremely hard to measure due to the < 1 mas to < 1 µas signal that even the closest planets would exhibit on their host stars. That being said, optical interferometry with its unparalleled angular resolution (see

Section 1.3) has been able to astrometrically confirm the presence of planetary companions [e.g. Hinkley et al., 2023], or has demonstrated that it can reach planetary astrometric signal precision [e.g. ARMADA Gardner et al., 2021]. Also of note is the *Gaia* spacecraft [Gaia Collaboration et al., 2016]; due to the unprecedented astrometric precision of this survey satellite, it has been predicted to detect between 20,000 and 70,000 planets once it has a sufficient observation baseline [Perryman et al., 2014]. This would propel the astrometric detection method to be by far the most productive of all detection techniques. Gaia will likely detect many Jupiter-like planets in potential Earth-Jupiter systems, including their inclinations; complementing Earth-like planet characterisations using the methods outlined earlier. This is especially important as the bulk and atmospheric composition of the Earth relates to its accretion history, and the effect of Jupiter on mediating the amount of water and carbon-rich material that formed it [O'Brien et al., 2014].

Now, while all of these techniques, particularly the radial velocity and transiting method, have been very successful in finding planets, these all detect planets indirectly. That is, most of them cannot provide us with spectra or direct radiation that will allow us to look for biosignatures (with the exception of transmission spectroscopy, though as mentioned that has problems of its own). Furthermore, they are rather biased towards larger planets or planets closer to their stars than Earth, as seen in Figure 1.1. Ideally, the best way to obtain a planetary spectrum would be to directly image the reflected light or thermal radiation emitted by the planet, which is what I explore in the next section.

1.2 The Direct Detection of Exoplanets

1.2.1 A Problem of Contrast

While direct imaging has been accomplished for a number of planets (see Figure 1.1 and Table 1.1), there are a number of factors that make this technique exceedingly difficult, and induces biases against terrestrial, Earth-sized exoplanets in the habitable zone of their star.

The first is a problem of contrast: a planet is many orders of magnitude fainter than that of its host star. This can be easily seen in Figure 1.5, where

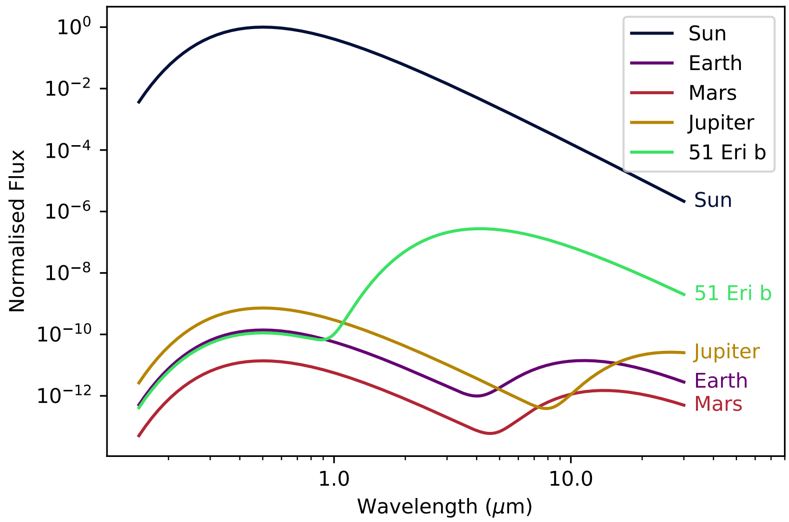

Figure 1.5: Fluxes of solar system planets, normalised to the solar flux. Solar system albedos and temperatures taken from Williams [2022, 2023]. Also included is a hot (700 K), young, Jupiter-sized planet based on the parameters of 51 Eridani b from Macintosh et al. [2015]. Figure adapted from Galicher & Mazoyer [2023].

the synthetic flux of various solar system objects is plotted against that of the Sun, normalised to the peak of the Solar radiation. Also plotted for comparison is a planet based on the parameters of 51 Eridani b [Macintosh et al., 2015], being a substantially younger, and thereby hotter, exoplanet that was successfully imaged with the Gemini Planet Imager [Macintosh et al., 2014].

A few things are notable here. Firstly, the planet flux is made up of two components: reflected and thermally emitted radiation. The former comes from the solar radiation reflecting off the planet's surface, clouds or atmosphere; a scaling of the solar radiation based on planet radius (R_p), distance from the sun/star (a) and Bond albedo (A). Normalised to the stellar flux, this is approximated by:

$$F_{\text{ref}}(\lambda) = \frac{A}{4}\left(\frac{R_p}{a}\right)^2 \frac{B(\lambda, T_{eff})}{\text{Max}(B(\lambda, T_{eff}))}, \tag{1.3}$$

where $B(\lambda, T_{eff})$ is the Planck function for a black body of temperature T_{eff}. Here, T_{eff} refers to the temperature of the star. For a solar-type star, this reflected component peaks in the optical part of the spectrum. I emphasise that this is an approximation where the albedo has no wavelength-dependence.

The second component, the thermal emission, is approximated by the black-body radiation of the planet itself:

$$F_{\text{ther}}(\lambda) = \left(\frac{R_p}{R_s}\right)^2 \frac{B(\lambda, T_{p,eff})}{\text{Max}(B(\lambda, T_{eff}))}, \tag{1.4}$$

where R_s is the stellar/solar radius and $T_{p,eff}$ is the planet's effective temperature. This emission generally peaks in the infrared. The surface temperature of the planet may in fact be higher than the effective temperature due to atmospheric processes hindering the emissivity of thermal radiation such as the greenhouse effect and clouds; as an approximation of the emission, this distinction is neglected. For the plot in Figure 1.5, planetary parameters were obtained from Williams [2022, 2023].

Regardless of the type of planetary radiation being detected, it is very clear that the star outshines its planets by a huge margin: ten orders of magnitude for an Earth-like exoplanet around a solar-type star in the visible part of the spectrum. For this reason, high-contrast imaging techniques are needed to reduce the emission of the star to better see the radiation of a planet. These come in two flavours: coronagraphy, and nulling interferometry.

Coronagraphy is a technique that involves masking the light from the star through the use of a focal plane mask that may come in the form of an opaque circular mask (a classical Lyot coronagraph), or other more complex designs such as the four-quadrant phase mask coronagraph [e.g. Rouan et al., 2000] and the vortex coronagraph [e.g. Foo et al., 2005]. In this manner, on-axis light from a star is blocked or diffracted out of view of a following pupil stop, while off-axis light remains [Galicher & Mazoyer, 2023]. Almost all high-contrast imaging instruments employ some form of coronagraphy, mostly in the near infrared, including VLT/SPHERE [Beuzit et al., 2019], Subaru/SCExAO [Jovanovic et al., 2015] and the Gemini Planet Imager (GPI) [Macintosh et al., 2014]. Multiple space telescopes have coronagraphic modes as well, including the Hubble Space Telescope [Grady et al., 2003], James Webb Space Telescope [Girard et al., 2022; Boccaletti et al., 2022] and, perhaps most impressively, the upcoming *Roman* Space Telescope's Coronagraphic Instrument (CGI) with a

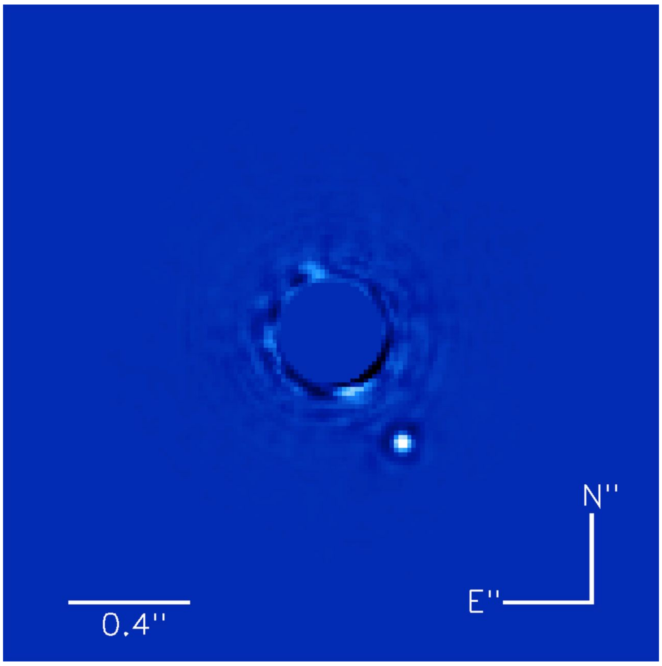

Figure 1.6: Stacked 30 minute image of the Beta Pictoris system after angular differential imaging (ADI), taken with the Gemini Planet Imager (GPI) instrument. From Macintosh et al. [2014].

planned contrast close to 10^{-8} [Kasdin et al., 2020]. An example of a coronagraphic image of the Beta Pictoris system, taken with GPI, is shown in Figure 1.6 [Macintosh et al., 2014]. It should be noted, however, that the focal plane mask can have a large angular size; Beta Pictoris lies at a distance of 19.4 pc, and Beta Pic b in the image is located at a separation of 9 AU [Macintosh et al., 2014]. This is the rough equivalent of imaging Jupiter in a solar system analogue from a distance of 10 pc. Thus planets that are further out from their stellar host are easier to image.

There are fundamental limitations to coronagraphs, however. The biggest limitation is that of the tradeoff between the inner working angle (IWA), the separation where the coronagraph throughput is at 50% [Galicher & Mazoyer, 2023]; the stellar angular diameter; and that of the contrast performance. The IWA is generally a few factors larger than the diffraction limit of the telescope itself ($\theta \approx \lambda/D$) [Boccaletti et al., 2015]. It has been shown by e.g. Guyon et al. [2006]; Belikov et al. [2021] that a coronagraph cannot fully suppress the light of a star, and that the more the light is suppressed, the greater the inner working angle is required to be. For the technically challenging task of imaging very close-in terrestrial planets around nearby bright solar-type stars, all three parameters of this tradeoff are required to be maximised and is thus a considerable issue. Current coronagraphic designs have not yet reached the fundamental tradeoff boundary yet, with the best known performances coming from the Decadal Survey Testbed, producing a 4×10^{-10} contrast at 3-9 λ/D IWA [Seo et al., 2019], or the 5×10^{-8} contrast at 2 λ/D produced by a testbed at the NASA Ames Research Center Belikov et al. [2010]. New testbeds demonstrating even more aggressive contrasts at smaller IWAs are being developed as well [Belikov et al., 2018; Walter et al., 2022, e.g.].

Furthermore, coronagraphs are extremely sensitive to wavefront errors and aberrations, due to these errors appearing as "speckles" that mimic point sources (such as planets). In general, most coronagraphs use adaptive optics, where a deformable mirror is used to correct the wavefront [see e.g. Babcock, 1953; Hardy, 1998], in order to minimise these errors. However, at the 10^{-10} contrast level, in order to reduce the speckle noise such that the planet is detectable, the root-mean-squared (RMS) path-length error on ground-based telescopes must be corrected down to a level of 10-100 pm, and at speeds of 10-100 kHz [Stapelfeldt, 2006; Galicher & Mazoyer, 2023]. These requirements are orders of magnitude from the current state of the art, such as the SPHERE eXtreme Adaptive Optics system (SAXO/SAXO+; Focardi et al. [2015]; Stadler et al. [2022]), or the Subaru Coronagraphic Extreme Adaptive Optics system (SCExAO; [Jovanovic et al., 2015]), which exhibit RMS path-length errors on the order of tens of nanometres and run at a few kHz. In fact, it has been posited that high contrast imaging has an ultimate limit of 10^{-8} from the ground [Stapelfeldt, 2006]. This can be alleviated by going above the atmosphere and into space, where turbulence induced speckles are minimised; precisely the domain of the future *Roman*/CGI [Kasdin et al., 2020] and Habitable Worlds Observatory (HWO) [National Academies of Sciences, Engineering, and Medicine, 2021; The LUVOIR Team, 2019] missions.

The other technique is nulling interferometry. There is only one active nulling interferometric instrument at present: the NOMIC instrument on the Large Binocular Telescope Interferometer (LBTI) [Hinz et al., 2016]. However, there is also ongoing work to develop a visitor instrument for the Very Large Telescope Interferometer (VLTI), named Asgard-NOTT (previously Hi-5) [Defrère et al., 2018a; Laugier et al., 2023], that will be a nulling interferometer with spectrographic capabilities working in the L′ band (3.5-4 μm).

A plot of the contrast levels for a few planetary archetypes (an Earth around a solar-type star, a Jupiter around a solar-type star, a 51 Eridani b analogue [Macintosh et al., 2015] around a solar-type star, and a Proxima Centauri b analogue around an M-dwarf star [Brugger et al., 2016; Del Genio et al., 2019, assuming $R_p \approx 1R_E$]) is shown in Figure 1.7. Overplotted are the achievable detection contrasts (after post-processing) that have either been recorded or predicted for a non-exhaustive list of high-contrast instruments. The instruments are separated into three broad catagories: current instruments (JWST/MIRI [Boccaletti et al., 2015, 2022], Gemini/GPI [Macintosh et al., 2014] and LBTI/NOMIC [Mennesson et al., 2016; Ertel et al., 2022]), near-future instruments (VLTI/NOTT [Laugier et al., 2023], *Roman*/CGI [Kasdin et al., 2020] and ELT/METIS [Carlomagno et al., 2020]), and far-future instruments. The two far-future instruments, the Habitable Worlds Observatory (HWO) [National Academies of Sciences, Engineering, and Medicine, 2021; The LUVOIR Team, 2019] and the Large Interferometer For Exoplanets (LIFE) [Quanz et al., 2022; Ranganathan et al., 2022] are two large-scale missions that have been recommended by National Aeronautics and Space Administration (NASA) and European Space Agency (ESA) panels respectively, and will be discussed at the end of this section.

As an aside, I note that the contrast requirement for LIFE is not yet defined, and as such the value of 10^{-8} was estimated from the the design specifications of the Nulling Interferometer Cryogenic Experiment (NICE) [Ranganathan et al., 2022]: a raw contrast of 10^{-5} to 10^{-6}, and further starlight suppression with post-processing techniques of a few orders of magnitude. These are in turn derived from the Terrestrial Planet Finder Interferometer (TPF-I) specifications and results from the Planet Detection Testbed (PDT) [e.g. Martin et al., 2012]. As with LIFE itself, these will be discussed later in this chapter. The main takeaway message from this plot is that all current and most near-future instruments just do not have the ability to reach the contrasts necessary for a terrestrial planet detection around a solar analogue.

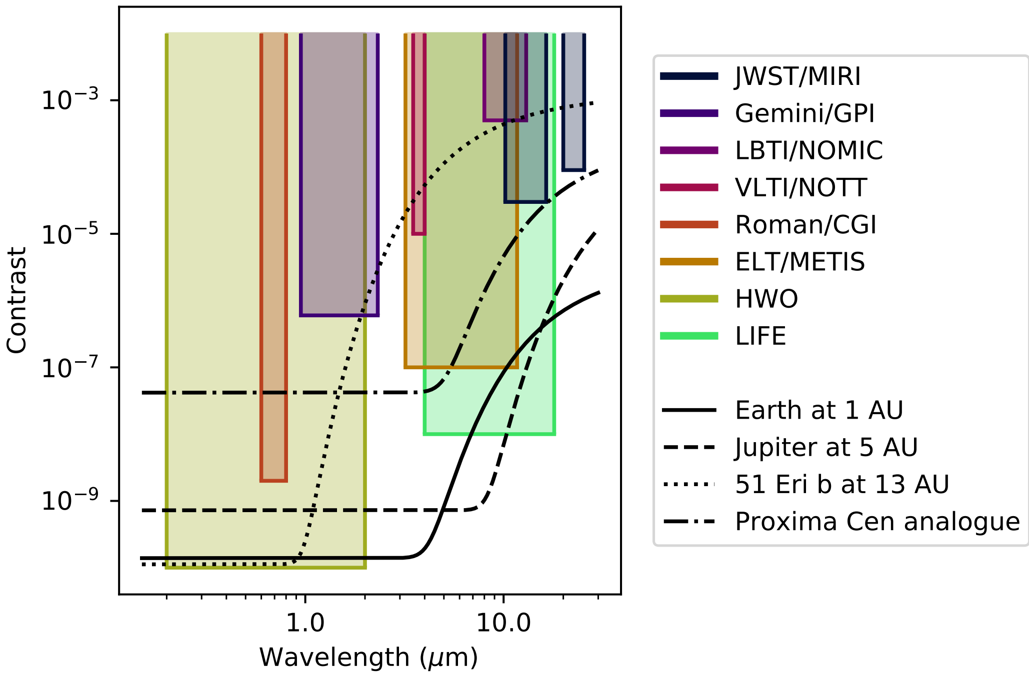

Figure 1.7: Contrast between a planet and its host star as a function of wavelength for four planetary archetypes: an Earth around a solar-type star, a Jupiter around a solar-type star, a 51 Eridani b analogue [Macintosh et al., 2015] around a solar-type star, and a Proxima Centauri b analogue around an M-dwarf star [Brugger et al., 2016; Del Genio et al., 2019, assuming $R_p \approx 1R_E$]. Overplotted are the contrast limits of a non-exhaustive selection of direct imaging instruments. References for each instrument are as follows: JWST/MIRI: [Boccaletti et al., 2015, 2022], Gemini/GPI: [Macintosh et al., 2014], LBTI/NOMIC: [Mennesson et al., 2016; Ertel et al., 2022], VLTI/NOTT: [Laugier et al., 2023], *Roman*/CGI: [Kasdin et al., 2020], ELT/METIS: [Carlomagno et al., 2020], HWO: [National Academies of Sciences, Engineering, and Medicine, 2021; The LUVOIR Team, 2019], LIFE: [Quanz et al., 2022; Ranganathan et al., 2022]. Note that JWST/MIRI has two regions in the top right-hand corner.

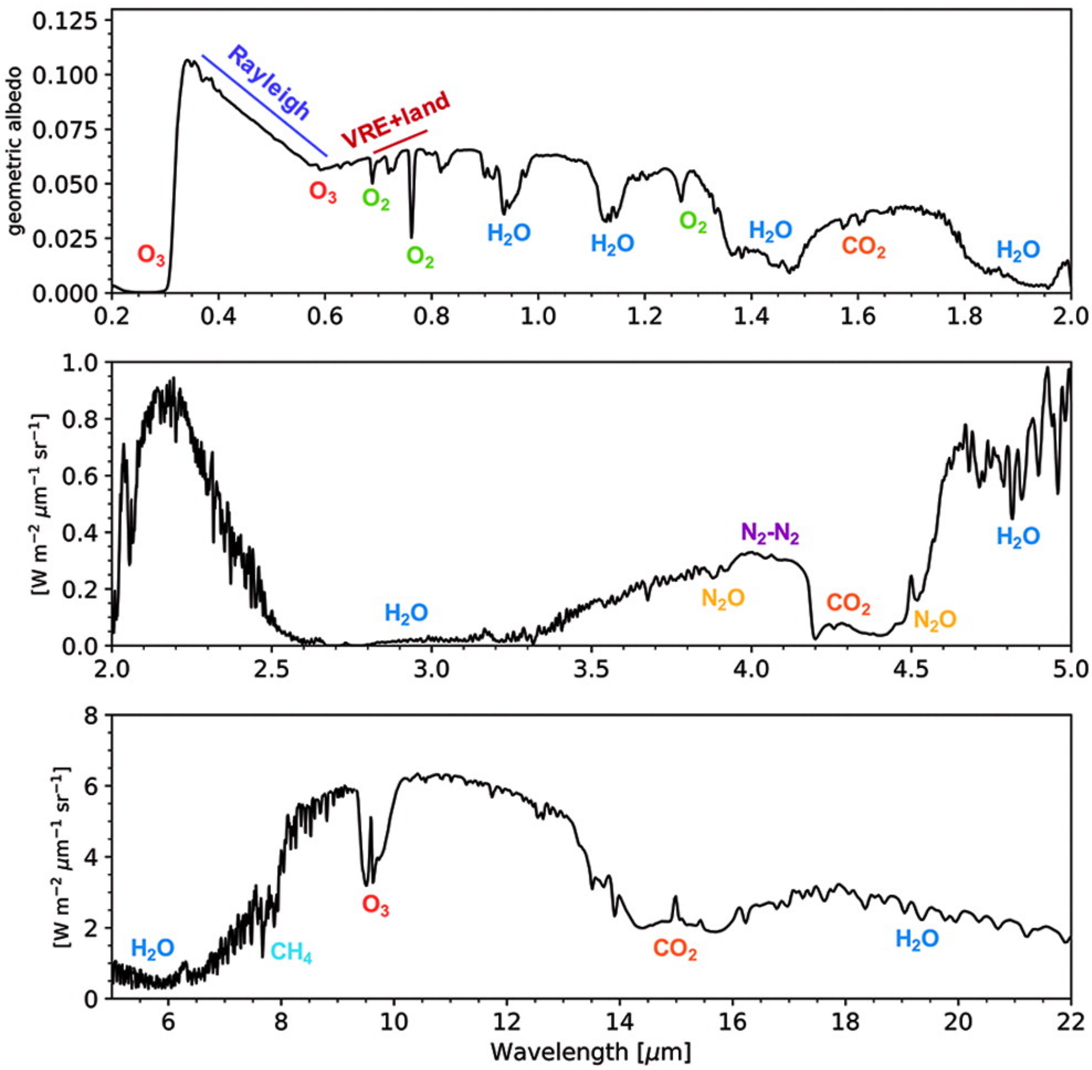

Figure 1.8: Key molecular absorption features of a synthetic Earth-like radiance spectrum, from Schwieterman et al. [2018]. Plotted in terms of geometric albedo for the visible and spectral radiance for the near/mid infrared. Note the relative abundance of different species in the infrared compared to the visible part of the spectrum.

1.2.2 The Gold Mine of the Mid-Infrared

It is clear from Figure 1.7 that the contrast is best for big, hot planets, and that the contrast requirements for terrestrial planets in the HZ are extremely demanding in the visible portion of the spectrum. However, it is also clear that the contrast is much more favourable in the mid-infrared (MIR): the solar radiation decreases while the planetary thermal emission peaks. The MIR regime also provides other benefits, specifically regarding biosignatures. Spectral signatures of key molecules such as H_2O, CO_2, O_3, N_2O and CH_4 among others can be located in the MIR (see Figure 1.8), providing insight into the planet's habitability [e.g. Catling et al., 2018; Defrère et al., 2018b]. Other advantages include being less affected by clouds than in the visible [e.g. Kitzmann et al., 2011; Konrad et al., 2022], and being able to constrain the radius that is otherwise degenerate with the albedo in the visible regime [e.g. Line et al., 2019; Carrión-González et al., 2020]. This can thus lead to a direct estimation of the surface temperature.

Unfortunately, there is another problem that arises in trying to observe planets in the MIR, specifically from the ground. In particular, the thermal background radiation from the sky, as well as radiation from the local telescope facility, peaks at these wavelengths (as Earth itself is an Earth-like exoplanet!), leading to prohibitively long integration times around even the closest stars [Defrère et al., 2018b]. For comparison, the ground-based thermal background in the MIR is seven orders of magnitude higher than the dominant space-based zodiacal light background [see e.g. Leinert et al., 1998; Otárola et al., 2015]. Furthermore, key biosignature absorption features will generally be inaccessible from the ground due to our own atmosphere absorbing these same features. For these reasons, if one wants to observe the MIR spectrum from HZ terrestrial planets, we must choose one of two methods: restrict ourselves to fairly narrow atmospheric windows that are both transmissive and less thermally emissive (known as the M and N bands) while employing cryogenic techniques to minimise the thermal background, or put our telescopes above the atmosphere and into space.

The former is the choice of the first generation instrument for the European Extremely Large Telescope (ELT), METIS (Mid-infrared ELT Imager and Spectrograph) [Carlomagno et al., 2020]. METIS will be able to observe planets in the L, M and N atmospheric bands, and will utilise a cryostat to minimise the number of components that are emitting at MIR wavelengths. It also utilises a cold-chopping mirror to quickly switch between on-target and sky observations, to calibrate the atmospheric background contamination. Together, this will make METIS one of the best performing MIR instruments available on the ground. From Figure 1.7, we can see that it will begin to detect Earth-like exoplanets around solar stars. Nevertheless, achieving the predicted contrast will be very difficult from the ground due to the aforementioned coronograph wavefront sensitivity, and METIS will still require extremely long integration times due to the thermal background generated from non-cryogenic optical surfaces.

Space telescopes are perhaps the more obvious choice, as once above the atmosphere one does not have to worry about the atmospheric background at all. The James Webb Space Telescope (JWST) carries a MIR instrument MIRI (Mid-InfraRed Instrument), that also functions as a coronagraph [Boccaletti et al., 2015, 2022]. This instrument has shown to have impressive sensitivity [Glasse et al., 2015], but unfortunately the coronagraph will not reach the contrasts necessary to uncover many planets other than warm and hot Jupiters. Furthermore, the MIRI coronagraph does not contain a spectrograph (and hence can only provide images and photometry of exoplanets), and also suffers from limited angular resolution.

Indeed, while the discussion currently has been focused on minimising the contrast requirements to observe terrestrial exoplanets, the concurrent problem of angular resolution is another issue that must be discussed and addressed.

1.2.3 A Problem of Angular Resolution

As I pointed out when discussing the Beta Pictoris system, direct imaging techniques work best when the planets are at large angular separations from their host stars. This is due to a combination of ensuring the star and planet can be resolved by the telescope being used, as well as the fact that high-contrast imaging techniques can achieve deeper contrasts further away from the star.

Unfortunately for terrestrial planet hunters, the angular separation between an Earth-like exoplanet around a solar-type star as close as 10 pc is much smaller than that of systems such as Beta Pictoris. This then requires the use of even larger telescopes than current facilities in order to increase the achievable angular resolution. In Figure 1.9, the angular separation of planetary archetypes (an Earth (a = 1 AU) at 5 pc, an Earth (a = 1 AU) at 10 pc, a Jupiter (a = 5 AU) at 10 pc, and a Proxima Centauri b analogue (a = 0.05 AU [Brugger et al., 2016]) at 5 pc) is compared to that of the maximum angular resolution for the same high-contrast imaging instruments as Figure 1.7. Note that for coronagraphic instruments, I have calculated the achievable angular separation as their IWA. As described earlier, this value does not correspond to the maximum contrast, which is generally achieved at a larger angular separation. Fundamentally, the Figures 1.7 and 1.9 should be combined into one three-dimensional plot, but this is difficult to display visually. For interferometric instruments, the achievable angular separation is given by the wavelength divided by the separation between two apertures, known as the baseline, B ($\theta \approx \lambda/B$).

We can see that the next generation of extremely large telescope instruments, such as METIS on the ELT, will achieve the angular resolution required to analyse a few terrestrial exoplanets, but is hampered due to the use of the MIR (which suffers from poor angular resolution). Of course, one could instead look in the visible regime with much better angular resolution, but then we run into the issues of contrast discussed earlier. A nulling interferometer such as Asgard/NOTT should achieve the angular resolution required for most planets due to an interferometer's ability to achieve an angular resolution based on the distance between its apertures rather than the diameter of its collectors. Unfortunately though, it is severely limited by the contrast requirements in the L′ band.

The key way to break this barrier is to combine the resolution benefits of a nulling interferometer with the sensitivity benefits of a MIR space telescope. That is to say, a MIR nulling space interferometer. This is precisely the definition of the Large Interferometer For Exoplanets (LIFE) mission [Quanz et al., 2022], and the eventual endpoint of the research that has been conducted in this thesis. As seen in Figures 1.7 and 1.9, this concept is one of the few observatories capable of viewing the tiny angular separation demanded by Earth-like exoplanets at distances beyond 10 pc, as well as HZ planets

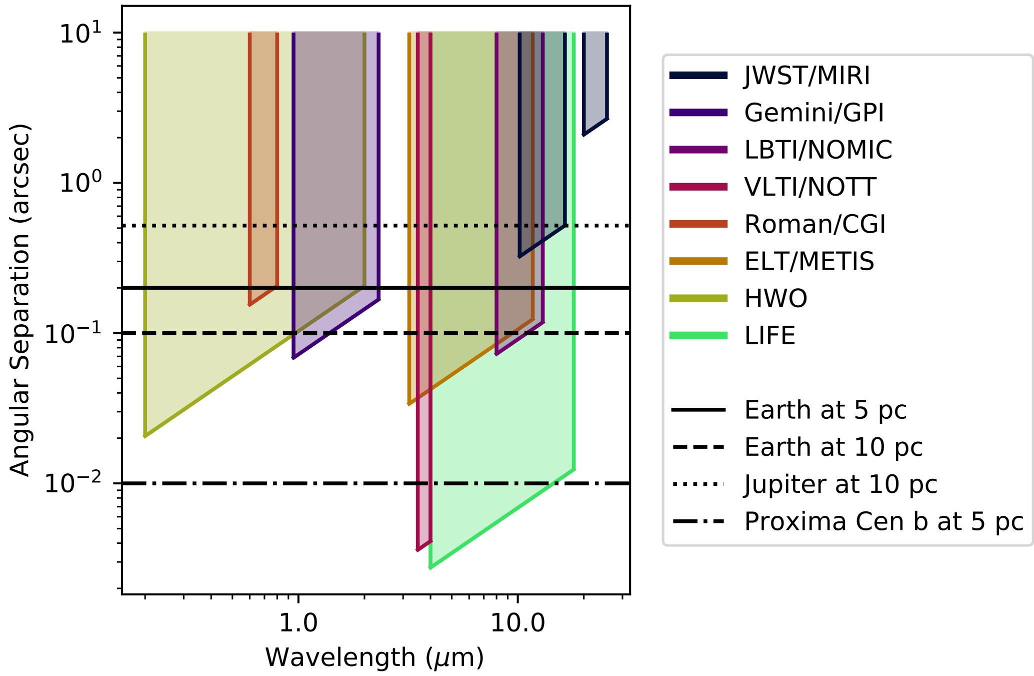

Figure 1.9: Angular separation between a planet and its host star as a function of wavelength for four planetary systems: an Earth (a = 1 AU) at 5 pc, an Earth (a = 1 AU) at 10 pc, a Jupiter (a = 5 AU) at 10 pc, and a Proxima Centauri b analogue (a = 0.05 AU [Brugger et al., 2016]) at 5 pc. Overplotted are the angular resolution limits (IWA for coronagraphs, maximum baseline resolution for interferometers) of a non-exhaustive selection of direct imaging instruments. References for each instrument can be found in Figure 1.7. As with Figure 1.7, JWST/MIRI has two regions in the top right-hand corner.

around M-dwarfs. To summarise why a MIR nulling space interferometer is ideal:

- A MIR mission, so that we can minimise the contrast required to find and characterise terrestrial planets in the HZ.
- A space mission, so that we can remove the problems associated with observing in the MIR from the ground.
- Interferometry, so that we can achieve huge baselines providing unparalleled angular resolution compared with a monolithic aperture, especially at MIR wavelengths. This also greatly reduces the cost of sending such a large monolithic aperture to space.

Before we continue, I want to mention the Habitable Worlds Observatory (HWO), which is the current name of the large ultraviolet/visible/infrared space telescope endorsed by the US Astro2020 decadal survey as a successor to JWST [National Academies of Sciences, Engineering, and Medicine, 2021]. This observatory is designed to be a middle ground between the mission concepts of LUVOIR (Large UltraViolet Optical InfraRed surveyor) [The LUVOIR Team, 2019] and HabEx (Habitable Exoplanet Observatory) [Gaudi et al., 2019], with one of its primary objectives to "provide a robust sample of approximately 25 atmospheric spectra of potentially habitable exoplanets" [National Academies of Sciences, Engineering, and Medicine, 2021]. In order to achieve this, it will harness the power of the shorter-wavelength portion of the spectrum to achieve close to the high angular resolution available from an interferometer using a 6 m telescope (see Figure 1.9). Concurrently, it will also aim to achieve a coronographic contrast of 1×10^{-10}, allowing it to separate the light from a terrestrial Earth-like planet from a solar-type star. There is currently no detailed mission concept, but if after the current pre-phase A studies show that reflected light spectra of 25 Earth like planets can be measured, then it could be a valuable mission for biosignatures.

Nevertheless, HWO does have multiple downsides compared to a mission like LIFE. First, the shorter wavelengths used are inferior to the MIR for the reasons listed in Section 1.2.2, primarily among which is the relatively fewer atmospheric biosignatures present shortwards of the MIR and the inability to measure a radius. One specific example is that of O_3, which when paired with CH_4 is a potent biosignature [Schwieterman et al., 2018; Konrad et al., 2022]. LIFE will have easy access to a relatively strong O_3 feature at 9.65 µm, whereas HWO must contend with the so "Huggins bands" at around 300 nm, which while very sensitive to O_3 and by proxy O_2, are very difficult to access due to the short wavelengths. While HWO will have access to the Fraunhofer A O_2 feature, it has been shown that O_3 is able to be detected at significantly lower concentrations of O_2 [e.g. Des Marais et al., 2002; Reinhard et al., 2017; Schwieterman et al., 2018; Defrère et al., 2018b], which is especially important for terrestrial planets with atmospheres akin to the early Earth [Schwieterman et al., 2018; Alei et al., 2022]. Secondly, the cost estimate of HWO is around $11B USD (2020) [National Academies of Sciences, Engineering, and Medicine, 2021], which is comparably more than that of the LIFE mission (approximately $2B USD [Cockell et al., 2009, adjusted for inflation]). The main upside is that there are a number of space coronagraphs already in space (e.g. JWST Boccaletti et al. [2022]) and planned (e.g. *Roman* Kasdin et al. [2020]), unlike space interferometry.

That being said, the very different wavelength bandpasses of LIFE and HWO lead them to being complementary to each other, rather than being put in direct competition. In particular, a reflected light mission like HWO will be able to constrain the properties of a planet's upper atmosphere, including clouds, for which a MIR mission is not very sensitive. Crucially, however, this should be combined with the radius and temperature constraints provided by a MIR such as LIFE; otherwise, HWO would be hindered by the albedo/radius degeneracy. Furthermore, a complete wavelength coverage from the optical to the MIR would allow insights into the energy budget of the planet, its surface temperature and even whether the greenhouse effect is present [e.g. Carrión-González et al., 2023]. The synergies likely extend to operational considerations, where if both missions were flown at similar times the identification of the best targets for in-depth follow up could be made more efficient, increasing the amount of operational time of both missions spent on characterisation [Beichman et al., 2023]. Ideally, both missions would be successful in launching (HWO by NASA, LIFE by ESA), leading to extraordinary leaps in our understanding of the habitability of other worlds.

1.3 Optical/IR Interferometry

The first discussion on how the interference of light could be used in astronomy to measure stars was by Fizeau [1868], which was then built upon by Michelson [1920] culminating in the first measurement of the diameter of a star, Betelgeuse, by the Mt Wilson 20 ft interferometer [Michelson & Pease, 1921]. Efforts to extend this interferometer to 50 ft were unsuccessful, but the technique was revived through the work of Labeyrie [1975], who measured fringes from Vega using distributed apertures. Since then, the field has extended leaps and bounds beyond where it started with Fizeau, with successful interferometric baselines up to 300 m regularly being used at the Center for High-Angular Resolution Astronomy (CHARA) array [ten Brummelaar et al., 2005].

The next few sections will provide a brief introduction to the theory of classical and nulling interferometry, before examining the history and developments made in the field of optical/infrared space interferometry. The mathematical derivation is adjusted from Hansen [2019], which in turn is based on Boden [2000] and Haniff [2007]. Further information regarding the history and development of interferometry can be found in Lawson [2000], Monnier [2003] and Eisenhauer et al. [2023], and more in-depth mathematical treatments can be found in Glindemann [2011], Labeyrie et al. [2014] and Buscher & Longair [2015a].

1.3.1 Interferometry Basics

An interferometer is essentially a physical manifestation of Young's double slit experiment [Young, 1807]. Consider plane monochromatic light waves of wavelength λ from a distant object, such as a star, incident on an aperture with two slits, separated by a distance B. The light will diffract, and the two diffracting electric fields (notated E_1 and E_2) interfere with each other, causing a sinusoidal pattern incident on the focal plane known as a "fringe". The angular spacing between two fringes is given by $\theta = \lambda/B$ [Born & Wolf, 1999].

Now, instead of two slits, consider two identical small apertures at positions $\mathbf{x_1}$ and $\mathbf{x_2}$, with the baseline between them being $\mathbf{B} = \mathbf{x_2} - \mathbf{x_1}$. Then,

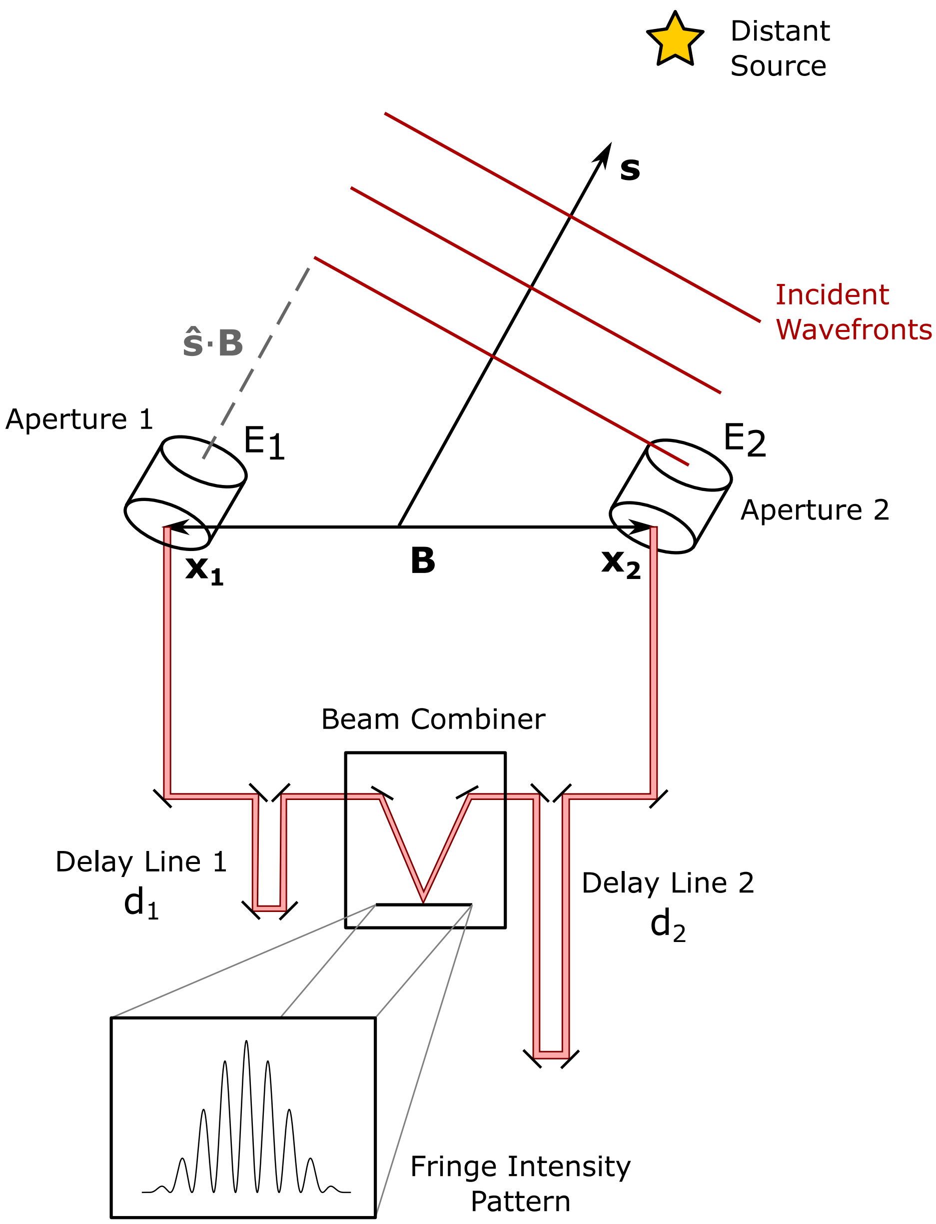

Figure 1.10: A simple interferometer setup. Here **B** represents the baseline of the interferometer, consisting of telescopes at $\mathbf{x_1}$ and $\mathbf{x_2}$. The position of the target star is denoted **s**, and d_1/d_2 are the two different optical paths (modified through delay lines).

suppose that they are looking at a point source with position $\mathbf{s}$. This setup is illustrated in Figure 1.10. Let each electric field be propagated through the two arms of the interferometer by different optical path lengths d_1 and d_2 respectively, right before the light from the two telescopes is combined. The detector measures the time averaged intensity of the superposition of the two incident electric fields, and so using the scalar field approximation, the detected intensity is proportional to:

$$i = \langle |E_1 + E_2|^2 \rangle \propto 1 + \cos\left(\frac{2\pi}{\lambda}(d_1 - d_2 + \hat{\mathbf{s}} \cdot \mathbf{B})\right). \tag{1.5}$$

The quantity $D = d_1 - d_2 + \hat{\mathbf{s}} \cdot \mathbf{B}$ is known as the optical path difference/delay (OPD) of the measurement, and it can be seen that the intensity will vary sinusoidally; equivalent to that of the fringes in Young's double slit experiment. The fringe pattern of an interferometer can be seen in Figure 1.10.

Let's now develop these concepts for an extended source. The brightness on the sky can be written as $I(\mathbf{s} = \mathbf{s_0} + \mathbf{\Delta s})$ where $\mathbf{s_0}$ is pointing towards the centre of the object and $\mathbf{\Delta s}$ perpendicular to this in the plane of the sky. We can assume that the extended source is just a number of point sources, and so we integrate the source intensity over the solid angle $d\Omega$ in the sky:

$$i(\mathbf{s_0}, \mathbf{B}) \propto \int I(\mathbf{s}) \left[1 + cos\left(\frac{2\pi}{\lambda} D\right)\right] d\Omega. \tag{1.6}$$

Haniff [2007] and Boden [2000] show that, assuming that the delays d_1 and d_2 are adjusted such that they cancel the geometric delay term $\mathbf{s_0} \cdot \mathbf{B}$ but still introduce a small path delay $D = \delta$ to one arm of the interferometer, the intensity can be written as:

$$i(\mathbf{s_0}, \mathbf{B}, \delta) = F\left(1 + \Re\left[\gamma e^{\left(-i\frac{2\pi\delta}{\lambda}\right)}\right]\right), \tag{1.7}$$

where F simply denotes the total flux obtained from the two apertures and γ is a quantity known as the complex coherence or complex visibility (sometimes notated as V, but this can be confused with the modulus of the complex coherence). The complex coherence, usually normalised to the total intensity, is the fundamental measurement of an interferometer and from Haniff [2007] is given by

$$\gamma = \frac{1}{F}\int I(\mathbf{\Delta s})e^{-i\frac{2\pi}{\lambda}(\mathbf{\Delta s}\cdot\mathbf{B})}d\Omega \tag{1.8}$$

$$\gamma(u,v) = \frac{1}{F}\int I(\alpha,\beta)e^{-2\pi i(\alpha u+\beta v)}d\alpha d\beta, \tag{1.9}$$

where α, β are angles on the sky (β in the direction of the north celestial pole) and u, v are spatial frequencies corresponding to the east B_E and north B_N components of the baseline:

$$u \equiv \frac{B_E}{\lambda} \qquad\qquad v \equiv \frac{B_N}{\lambda}. \tag{1.10}$$

Hence, the complex coherence can be interpreted as a sample from the two-dimensional Fourier transform of the source brightness distribution, and is a relationship commonly known as the van Cittert-Zernike theorem [van Cittert, 1934; Zernike, 1938]. A measurement of the complex coherence can be recovered to within a constant if $i(\mathbf{s_0}, \mathbf{B}, \delta)$ is measured at multiple delays δ. Furthermore if multiple measurements of γ can be taken on different baselines, theoretically it is possible to recover an image of the object. The equivalent angular resolution of an interferometer, therefore, is given by the maximum spatial frequency able to be sampled: $\theta = \lambda/B$.

Splitting the complex coherence into a modulus $V = |\gamma|$, simply known as the visibility, and phase ϕ component, we arrive at a detector intensity of:

$$i(\mathbf{s_0}, \mathbf{B}, \delta) \propto 1 + V\cos\left(\frac{2\pi\delta}{\lambda} + \phi\right). \tag{1.11}$$

Here, we see that the visibility simply affects the amplitude of the fringes, equivalent to the definition of the visibility by Michelson [1920]:

$$V = \frac{i_{\max} - i_{\min}}{i_{\max} + i_{\min}}, \tag{1.12}$$

and that the phase of the complex coherence is just the phase offset of the fringes from a defined centre point. The phase component encodes both information about the morphology of the astrophysical source, as well as delay offsets due to differing optical path lengths; the latter will be discussed in the following section. There are many ways to implement an interferometric beam combiner to recover these variables, and a discussion of this can be found in the literature [e.g. Buscher & Longair, 2015b; Hansen et al., 2022].

The previous discussion assumes monochromatic light; modern interferometers function with a finite spectral bandpass. Buscher & Longair [2015c] shows that for a rectangular response function over a bandpass $\Delta\lambda$ centred at a wavelength λ_0, the polychromatic intensity is proportional to:

$$i \propto 1 + \mathrm{sinc}\left(\frac{\delta\Delta\lambda}{\lambda_0^2}\right) V \cos\left(\frac{2\pi\delta}{\lambda_0} + \phi\right). \tag{1.13}$$

Hence, the polychromatic response simply modulates the fringes by a sinc function with a characteristic scale of $\Lambda = \lambda_0^2/\Delta\lambda$, known as the coherence length. In order to have maximum power in the fringes, the differential delay between the interferometer arms δ must be made as small as possible, while still being able to be modulated. As δ approaches Λ, the power decreases until falling to zero when the delay equals the coherence length. A schematic of this phenomena is found in Figure 1.11, where the coherence length is the position where the polychromatic fringe goes to zero.

1.3.2 The Turbulent Atmosphere and Fringe Tracking

Unfortunately, the derivation described in the previous section was for an ideal interferometer; on the ground one has to deal with the effects of the atmosphere. The atmosphere is turbulent, causing patches of air to vary randomly in temperature and pressure. As the temperature and pressure then affect the refractive index of air, this causes the light passing through to be disturbed, resulting in a corrugated wavefront and a phenomenon known as "seeing". Seeing will cause light observed by a telescope to have a phase offset that varies spatially and temporally. Interferometers are affected differently by atmospheric seeing compared to their monolithic cousins: whereas a single telescope will experience a loss in resolution, an interferometer will see a loss of sensitivity and coherence.

The strength of turbulence can be characterised spatially by the Fried parameter r_0, which determines the spatial scale at which the RMS phase variation caused by the atmosphere is 1 radian [Fried, 1966]. Hence in order to

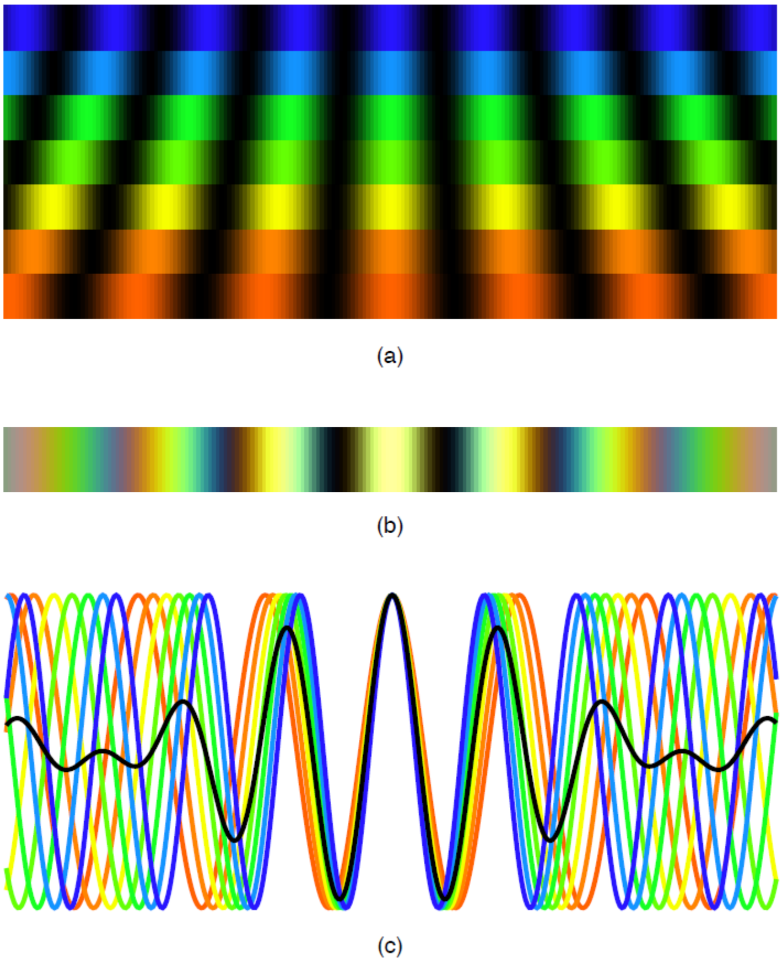

Figure 1.11: Polychromatic fringes. a) Fringes as seen at 7 single wavelengths. b) A polychromatic fringe generated by summing the single wavelength fringes. c) A cross section of the fringes, showing that the polychromatic fringe is modulated by a sinc function due to the differing responses of each component wavelength. Plot from Lawson [2000].

reduce the effect of seeing on the spatial wavefront, the telescope apertures should be less than r_0; otherwise, some form of adaptive optics is required. The effects can also be further reduced through the use of a spatial filter, such as a pinhole [e.g. Ireland et al., 2008; Lopez et al., 2022] or single-mode fibres [e.g. Coudé du Foresto et al., 1997; Coudé du Foresto et al., 1998]. In using such a filter, any high frequency modal noise in the wavefront caused by seeing is rejected, leaving behind a much purer beam profile that is free (or in the case of a pinhole, less distorted) from atmospheric corrugations [Buscher & Longair, 2015d]. The downside is that these filters, due to them rejecting aberrated light, will end up throwing away a significant portion of the incoming wavefront and results in a degrade in throughput. In essence, a spatial filter converts spatial phase errors over the aperture into intensity losses.

Nevertheless, this is generally a worthwhile tradeoff, as the varying intensity can be monitored by dedicated photometric channels [e.g. Coudé du Foresto et al., 1998] and calibrated out in post-processing. Even without photometric channels, there are still ways to estimate the intensity fluctuations and losses such as through estimating the time-averaged mean intensity of each arm [Shaklan et al., 1992], or through the use of an asymmetric fibre coupler [Monnier, 2001]. In theory, one could use the latter calibration concept on a coupler with a spectrally varying coupling ratio, where the estimator is applied to wavelengths of asymmetric coupling and interpolated to wavelengths of the coupler that are more balanced in output.

Perhaps more pertinent though is the temporal evolution of the turbulence. The frozen turbulence hypothesis states that most temporal variation is caused by the bulk motion of the atmosphere being blown by the wind [Taylor, 1938; Buscher & Longair, 2015d]. If there is only one layer of turbulence moving at a speed v, the phase variation can be characterised by the coherence time defined as [Roddier, 1981]:

$$t_0 = \frac{r_0}{v}. \tag{1.14}$$

For multiple layers, one can use an effective wind speed based on the weighted average of the different layers. This coherence time defines the timescale at which the phase changes by 1 radian, and is usually on the order of a few milliseconds [Buscher & Longair, 2015d]. Here we can see the main problem: one must take exposures on a timescale less than the coherence time to avoid the fringes from blurring due to the changing phase of the atmosphere. This means that far fewer photons will be obtained per exposure compared to the much longer exposures taken by single aperture telescopes.

The varying nature of the fringe phase due to the atmosphere means it is also impossible to recover the astrophysical phase component of the visibility with two apertures. There are techniques to recover a phase observable with more apertures, such as closure phase [e.g. Jennison, 1958; Baldwin et al., 1986; Monnier, 2000], which cancels out the atmospheric disruption by adding phases in a closed triangle, and differential phase [e.g. Petrov et al., 2007; Buscher & Longair, 2015d], but these observables will not be used in this thesis. Hence the main observable that can be recovered with a two aperture interferometer is the visibility V, or more precisely the squared visibility V^2.

This squared visibility can nonetheless provide useful information about the source. For example, if we consider a resolved uniformly-illuminated stellar disk on sky, the complex coherence is given by the two-dimensional Fourier transform:

$$\gamma(\mathbf{u}) = \mathcal{F}\left(\frac{1}{F}I(\sigma)\right) = \mathcal{F}\left(\mathrm{rect}\left(\frac{|\sigma|}{\theta_d}\right)\right) = 2\frac{J_1(\pi\theta_d|\mathbf{u}|)}{\pi\theta_d|\mathbf{u}|}, \tag{1.15}$$

where $\boldsymbol{\sigma}$ is the sky coordinate vector, $\mathbf{u}$ is the spatial frequency vector ($\mathbf{B}/\lambda$), θ_d is the angular diameter of the star and J_1 is the Bessel function of the first kind. Thus, taking the squared visibility:

$$V^2 = |\gamma(\mathbf{u})|^2 = 4\left|\frac{J_1(\pi\theta_d|\mathbf{u}|)}{\pi\theta_d|\mathbf{u}|}\right|^2. \tag{1.16}$$

Notably, if we make visibility measurements at various baselines, we can make a so called "visibility curve" where the only free parameter is the stellar angular diameter. Hence, using solely the visibility, we can resolve and recover the diameters of stars otherwise impossible to measure with single telescopes. Such a process was used by Michelson & Pease [1921], who measured the diameter of Betelgeuse by modifying the baseline of the Mt Wilson 20 ft interferometer until the fringes disappeared; finding the minimum of the above visibility function at $1.22\lambda/\theta_d$.

Though taking exposures with a duration less than a coherence time will prevent the fringes from smearing within one exposure, in order to achieve a high signal to noise, many exposures will have to be incoherently averaged together. This means that the temporal evolution of turbulence will still have to be corrected at some level. The effect of a phase error in the atmosphere can translate into an optical delay error in the interferometer (that is, light through some part of the atmosphere will travel slightly further than through another part), and so can be corrected with a delay line. This is a translatable stage that can quickly change the optical path inside of the interferometer to compensate for the error induced by the atmosphere (seen in Figure 1.10). This correction is a form of adaptive optics known as “fringe tracking” and comes in two flavours: phase tracking and group delay tracking. Both require the use of the recovered phase of the visibility. The following is based on Lawson [2000] and Buscher & Longair [2015e].

Phase tracking involves keeping the delay error to within one radian; that is, making sure that the fringes are within one wavelength of their position if the atmosphere was absent (where the visibility is maximum). A type of phase tracking is known as phase unwrapping, where the fringes are modulated (through a change in delay) fast enough such that the atmospheric errors are constant. This requires a modulation time of $\leq t_0/2$, and so is restricted to bright sources. However, with such a scheme, if one has a dedicated fringe tracking detector, the science detector can have longer exposures as the phase error will not influence measurements substantially.

Group delay tracking relies on the fact that the fringes at different wavelengths will have different periods. If one can disperse the light into different wavelength channels (creating a so called “channelled spectrum” [Lawson, 2000], one can then disentangle the delay where all the wavelength channels have equal intensity - this is the true location of zero delay, and the offset is due to the atmosphere. With this method, the disturbances can be followed without the requirement for keeping the error to within one wavelength, and instead the requirement becomes that one needs to keep the error to within the coherence length Λ. The downside is that group delay tracking does not follow the atmospheric phase, and so while science exposures can be incoherently combined, individual exposures are still limited to being less than a coherence time. While group delay tracking is vital for fringe tracking in ground-based interferometers, the absence of the atmosphere in space means that a space interferometer like LIFE should (and as described in Hansen et al. [2023a], is required to) use phase tracking to obtain minimal optical path difference residuals.

1.4 Nulling Interferometry

So far, the main topic of discussion has been centred around so called "classical" or "imaging" interferometry, but for terrestrial exoplanet detection and characterisation, we require an interferometric technique that can block out the light from the host star as is done with coronagraphy. Such a technique is dubbed "Bracewell" or "nulling" interferometry, named after Bracewell [1978] who first discussed the technique.

The concept of nulling interferometry is at first glance rather simple. Rather than having the arms of a two telescope interferometer interfere constructively at an OPD of zero, the path of one of the arms can be phase shifted by π causing destructive interference. This essentially creates a "null" at an OPD of zero, or alternatively if the interferometer is fringe tracking on an internal delay of zero, any light on axis will be nulled out. This can be seen in Figure 1.12. Of course, with the sinusoid nature of fringes, there will then be a constructive maxima at an angular offset of $\theta = \lambda/2B$ due to the slight increase in OPD of an off-axis source.

This theory is easily applied to a planetary system: if the interferometer points to an on-axis star, and has its baseline chosen such that the HZ of that star lies $\lambda/2B$ away from the star, then the host star light will be nulled and any off-axis HZ planet signal will be amplified through constructive interference. In the absence of noise and with a perfect instrument, simply detecting any flux at all is indication of a planet [Fridlund, 2002]. As Bracewell [1978] notes, however, there will still be unwanted noise and thus the signal needs to be modulated. The conceptually simplest modulation is a rotation about the optical axis: the stellar signal will remain constant, but the planet light will move in and out of constructive and destructive fringes (shown in Figure 1.13), thus allowing the planet signal to be extracted. The radial position of the planet is also encoded into the signal from the number of fringe crossings it makes.

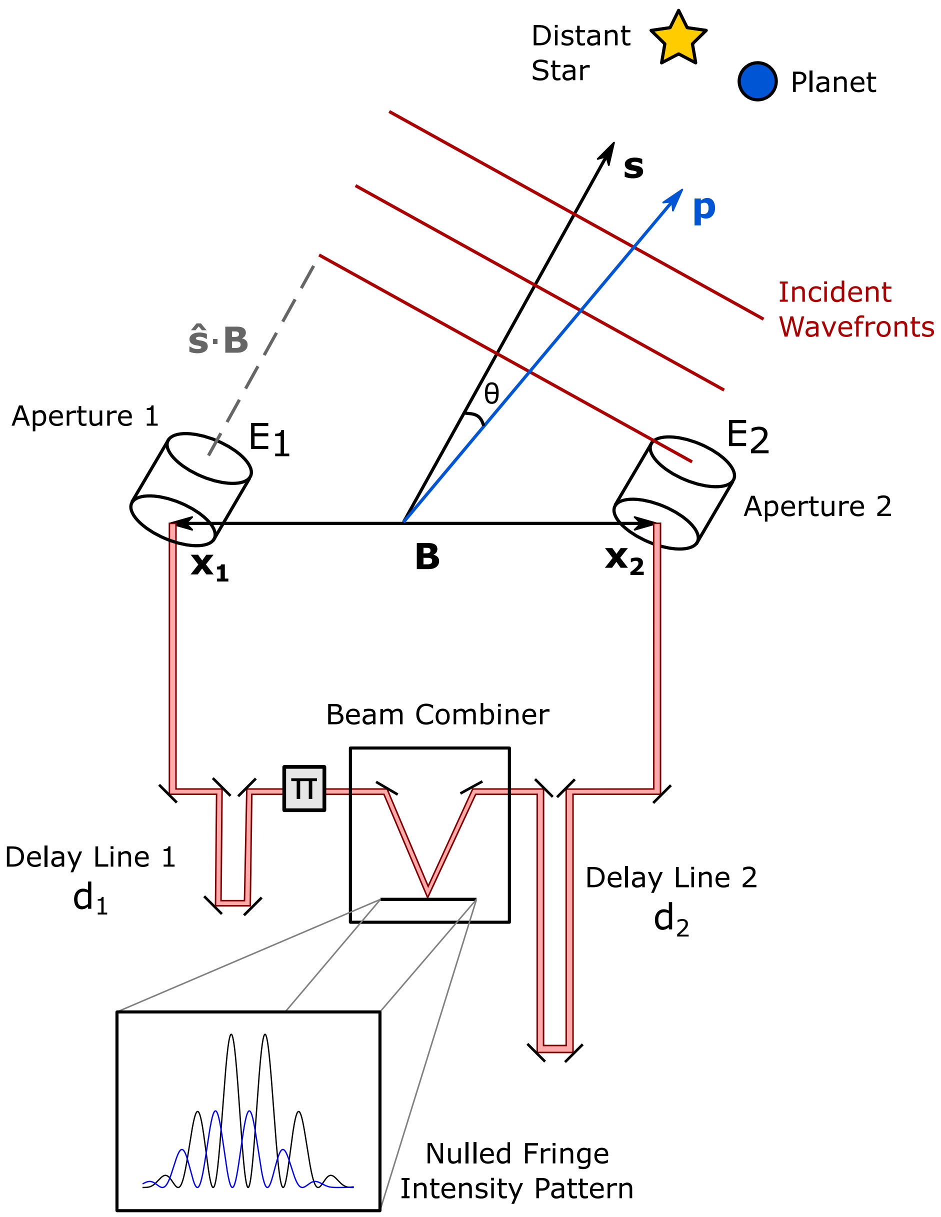

Figure 1.12: Schematic of a Bracewell nulling interferometer, modelled after Figure 1.10. The difference is the addition of a π phase shift in one arm, resulting in destructive interference for an on-axis stellar source. Any off-axis planet signal will encounter a small amount of geometric delay and thus the fringes will be phase shifted. Hence, at a delay of zero, the starlight is nulled but the planet light is transmitted.

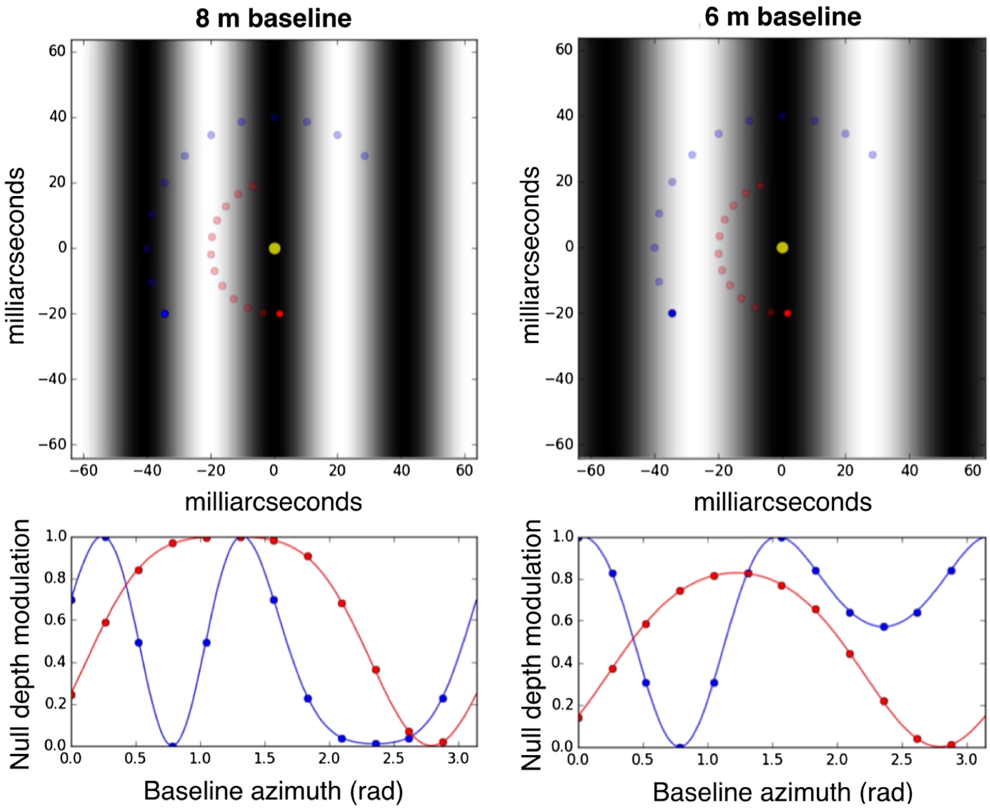

Figure 1.13: Top: Nulling interferometer transmission maps for two baselines; essentially a projection of the fringe pattern onto sky coordinates via the van Cittert-Zernike theorem (Equation 1.9). Overplotted are two planets in a planetary system with a simulated rotation of the array. Bottom: Transmission (or normalised null depth) as a function of azimuth angle for the two planets as the array rotates. It is apparent that planets at two different angular separations will produce different modulation signals. Taken from Lagadec et al. [2021].

In general, and as discussed more thoroughly in [Dannert et al., 2022; Hansen et al., 2022], there are a number of fundamental noise sources that such an interferometer must deal with, even if it is put in space, above the previously discussed atmospheric background and turbulence. First is the zodiacal light; scattered light from dust in the solar system that provides an inescapable background, especially at MIR wavelengths. Léger et al. [1996] and Fridlund [2002] point out that the zodiacal light at 10 μm would outshine a terrestrial planet by a factor of at least 400. Such a bright background requires some modulation to identify the signal, and in such a situation adds a DC bias to the signal extraction.

Stellar leakage is a noise term that is specific to nulling interferometry and is effectively the remaining stellar light that is not nulled. This is due to the fact that for an interferometer trying to sufficiently resolve a terrestrial planet in the HZ, a star close to Earth (where a terrestrial planet is most detectable) is a resolved disk rather than a point source. Hence the stellar limb will not be fully nulled and will contribute to the noise. Like with the zodiacal light, this is also a DC bias and can be removed through signal extraction after modulation.

However, as pointed out by Angel & Woolf [1997] and Mennesson et al. [2005], the stellar leakage from a Bracewell interferometer is severe and thus requires any fluctuations in the null to be minimised, monitored and accounted for on rapid timescales. An alternative is to add more telescopes to the configuration; Angel & Woolf [1997] first proposed one such idea, four non-identical telescopes in a row with non-identical shaped telescopes. Such a configuration allows for a much deeper and broader null: the transmitted intensity of the Bracewell scales with small angular offsets as θ^2, whereas the Angel & Woolf [1997] double linear Bracewell scales as θ^6, and thus greatly reducing the stellar leakage. Many array architectures have been compared, including both one-dimensional and two-dimensional arrays, and the shape and depth of the null strongly depends on the number of telescopes, their configurations and their baselines [see e.g. Mennesson & Mariotti, 1997; Lay et al., 2005; Lay, 2005; Absil, 2006; Guyon et al., 2013]. Non-symmetric arrays can also provide a constraint on the position angle of the planet. Some alternate configurations and their transmission maps (akin to Figure 1.13) are shown in Figure 1.14. Hansen et al. [2022] takes another look at some of these

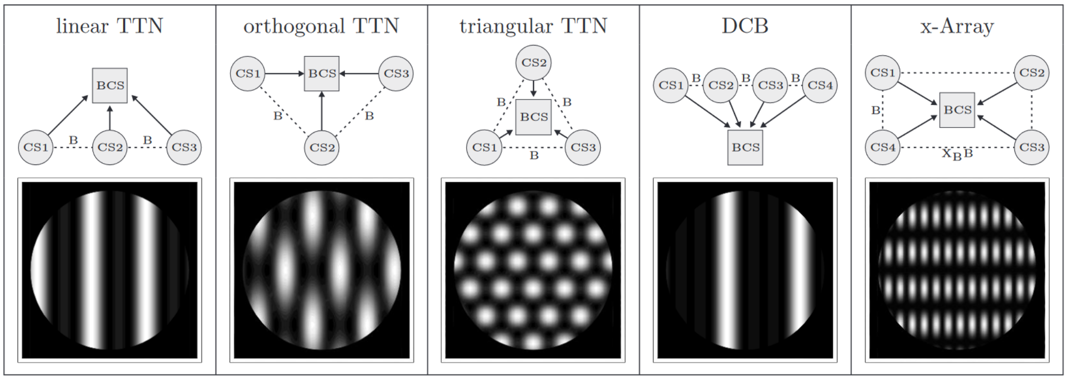

Figure 1.14: Various nulling interferometer configurations and their sky transmission maps. Acronyms: TTN - Three Telescope Nuller, DCB - Dual Chopped Bracewell, BCS - Beam Combiner Spacecraft, CS - Collector Spacecraft, B - Baseline, X_BB - Imaging Baseline. Taken from Wallner et al. [2006].

configurations in the light of some new developments in the field of nulling interferometery, namely kernel-nulling (see Section 1.5.2).

Finally, there is exozodiacal light around the exoplanet's host star that will also affect the planet signal, although if the emission is centro-symmetric (i.e. a face-on disk) then it will also be able to be removed by modulation. However, as described in Mennesson & Mariotti [1997] and Defrère et al. [2010], exozodiacal disks may not be centro-symmetric and may exhibit asymmetric clumps and/or disk offsets due to the presence of a planetary system. These features are deeply problematic for planetary extraction, and although sophisticated signal processing techniques may alleviate some of the constraints [e.g. Thiébaut & Mugnier, 2006; Defrère et al., 2010], it is critical that the nature of nearby exozodiacal disks are studied and those that are too inclined or too bright be removed from the catalogue of a future interferometer mission (like LIFE). Such studies are ongoing, including the HOSTS survey on the LBTI [Ertel et al., 2020] and a future survey for the upcoming VLTI/NOTT instrument [Defrère et al., 2018a].

While rotating the array in principle can modulate the planet signal and decouple it from the DC noise terms, in practice the rotation of the array will not be able to be modulated fast enough to account for any long term intensity fluctuations from any of the above sources, as well as infrared detector bias and gain instability [Mennesson et al., 2005; Defrère et al., 2010]. Because these noise sources are so much larger than the planet, fluctuations can easily mimic a planet signal and thus a faster modulation method is required. The current accepted method, described in Mennesson et al. [2005], is that of "internal modulation" or "phase-chopping": a rapid time-variable phase shift is applied to the outputs of two or more nulling interferometers (thus requiring a minimum of three telescopes if one aperture is shared). Since the pupil is real, then performing a $\pm\pi/2$ phase shift to each pair and differencing the resultant outputs will remove any centro-symmetric emission (that is, the zodiacal background, stellar leakage and a face on zodiacal disk) [Absil, 2006; Defrère et al., 2010]. In practice this can either be done simultaneously on two detectors or each one sampled alternatively on the same detector (hence the moniker "chopping") [e.g. Mennesson et al., 2005; Absil, 2006]. Because the phase-chopping can be performed much faster than a rotation, this process can reduce the impact of any fluctuations in these noise sources; and the removal of the symmetric emission means that these noise sources only contribute to the photon shot noise. Note here though, that while rotation of the array is not strictly required anymore when implementing phase chopping, in practice it is still required for good sky coverage and signal extraction properties [e.g. Lay, 2005; Absil, 2006].

1.5 Interferometry from Space

1.5.1 A Brief, Tragic History

After the seminal work of Bracewell [1978] and Bracewell & MacPhie [1979], the concept of nulling interferometry from space to observe exoplanets was studied in depth by both ESA and NASA, with the former listing it as a priority in the Horizon 2020 plan [Battrick, 1995]. Multiple conferences and workshops were held concerning the topic, and many mission concepts were formulated. These varied from connected element interferometers (such as putting the collectors on a boom), to free flying interferometers. These missions included but are not limited to: COSMIC [Traub & Carleton, 1985], FLUTE [Labeyrie et al., 1980], OASIS [Noordam et al., 1985], TRIO [Labeyrie et al., 1985] and SAMSI [Stachnik & Gezari, 1985], though none of these proposals reached a preliminary design review stage.

Eventually, two large missions were proposed around the turn of the century: NASA's Terrestrial Planet Finder-Interferometer (TPF-I) [e.g. Beichman et al., 1999; Martin et al., 2011] and ESA's *Darwin* mission [e.g. Léger et al., 1996; Kaltenegger & Fridlund, 2005; Cockell et al., 2009]. These were both free flying missions situated at the Earth/Sun L2 Lagrange point, and due to the similarities between the missions, both space agencies collaborated heavily. A majority of the research into nulling interferometry was conducted at this time: attempting to increase the technological readiness levels (TRLs) before launching these missions. This included the development of phase chopping mentioned in the previous section [Mennesson et al., 2005], as well as the development of the Planet Detection Testbed [Martin et al., 2012], which to date has the deepest recorded null of 6.5×10^{-7}. Achromatic nulls were also formulated at this time through the work of Peters et al. [2010] and the concept of the adaptive nuller, and one of the first "on-sky" nullers, the BracewelL Infrared Nulling Cryostat (BLINC) instrument, was developed and installed on the MMT and Magellan telescopes [Hinz et al., 2000; Hastie & McLeod, 2008].

Of particular note is the development of the "Emma X-array" configuration. Shown in Figure 1.15, the Emma X-array is the convergence of both ESA's [e.g. Wallner et al., 2006; Karlsson et al., 2006] and NASA's [e.g. Lay et al., 2005] studies into configurations: four telescopes in a rectangular formation, where the short end is the so called "nulling baseline", forming a two element Bracewell interferometer; and the long end is the "imaging baseline", where the two Bracewell interferometers are phase-chopped with a $\pm\pi/2$ phase shift. This design was chosen as the best tradeoff between stellar leakage/null depth, number of telescopes and instrument complexity among others [Lay et al., 2005; Karlsson et al., 2006; Lay et al., 2007]. Lay [2006] later found that the X-array should be stretched into a 6:1 imaging to nulling baseline ratio for better signal extraction. The "Emma" part of the Emma X-array, named after the wife of the mission's namesake "Darwin", refers to the beam combiner spacecraft being out of plane to the rest of the collecting spacecraft, thus allowing the collector beams to avoid being contaminated by the thermal emission radiating from each spacecraft [Karlsson et al., 2006]. This configuration remains the default configuration for the LIFE mission [Quanz et al., 2022], although this assumption is challenged in Hansen et al. [2022].

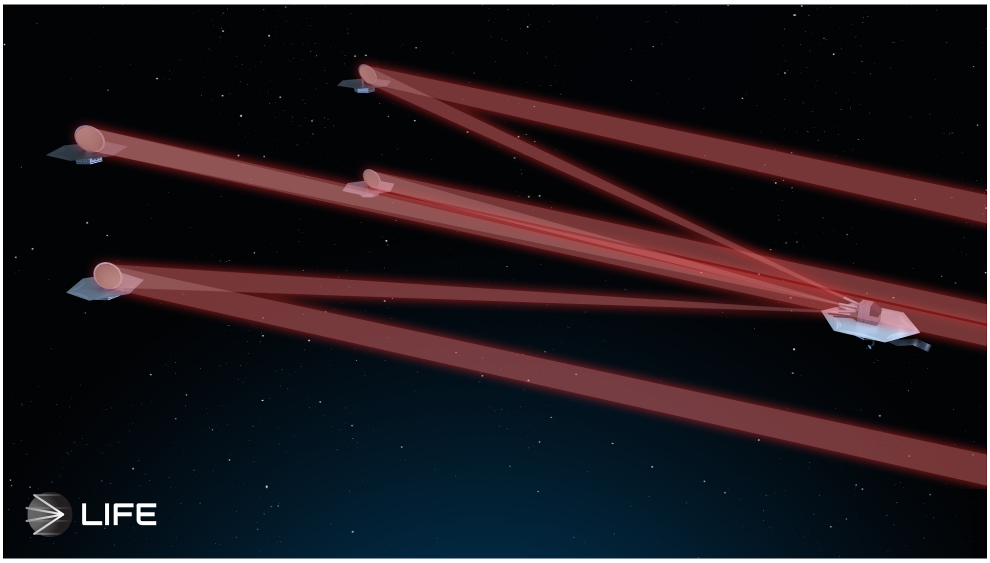

Figure 1.15: Artist's interpretation of the Emma X-array configuration. Used with permission from the LIFE Collaboration [2023].

A number of precursor missions were also planned to demonstrate some of the technologies needed for *Darwin*/TPF-I. These included the *Starlight* mission on the NASA side [Blackwood et al., 2003]: a two element imaging interferometer in an Earth-trailing orbit, operating in the visible and near infrared (NIR). While not demonstrating nulling, it would have demonstrated formation flying interferometry to a precision greater than the main mission due to the relative difficulty in maintaining formation in LEO. On the European side was the *Pegase* mission [Le Duigou et al., 2006]: a simple Bracewell interferometer, working between 2.5 and 5 μm, that would have demonstrated fringe tracking and nulling in a formation flying environment. Despite the relatively simple configuration of *Pegase*, it planned to use apertures of 40 cm, which would have made it a considerably sized mission in its own right.

Unfortunately none of these precursor missions were destined to launch, and furthermore the *Darwin* and TPF-I missions were nearly simultaneously removed from the recommended mission list of each of their relative agencies in the late 2000s. Why did these missions fail despite their huge scientific potential? Beichman et al. [2023] mentions a couple of factors: first there were the technical challenges and complexities involved with the missions. These interferometers were required to null starlight to a raw level greater than 1×10^{-6}; a daunting prospect for agency directors and funding bodies, especially at cryogenic temperatures (although this was demonstrated monochromatically by Martin et al. [2012] after the missions were cancelled). Furthermore, these missions require at least 4-5 telescopes in order to use phase-chopping, which is similarly concerning on the technological and budgetary standpoint compared to a monolithic aperture mission (such as *Roman*).

Second, and perhaps more critically, was the political aspect of the missions. In particular was the worry that the missions, for their size, were only catering to a single field of astrophysics; namely exoplanet research. Other similarly sized missions, such as JWST at the time of *Darwin*'s cancellation [Mather, 2005], catered to a much broader range of astrophysics research and thus enjoyed more widespread community approval. Of course, we also must consider the context of the time: the Global Financial Crisis was ongoing, leading to massive budget cuts. From the US perspective, JWST was ramping up and requiring as many resources as possible to ensure launch; thus any other large and technically challenging missions were swept aside in order to prioritise JWST. Regardless of the reasons why, the death of these mission concepts dealt a heavy blow to the nulling (in particular space-based nulling) interferometry community.

1.5.2 A Renewed Push

Despite the failures and missed opportunities in the past, at present there is now a resurgence of interest in space interferometry, notably through the LIFE collaboration [LIFE Collaboration, 2023]. This is an initiative to resurrect the *Darwin* mission concept as a MIR space interferometer with the main purpose of finding terrestrial in the HZ of nearby stars. A white paper detailing the opportunities of such a mission was submitted to the ESA Voyage 2050 plan [Quanz et al., 2021], and resulted in the plan labelling the "characterisation of the atmosphere of temperate exoplanets" as one of the proposed large class missions in the coming decades, with the condition of proving that such a mission could achieve its goal of characterising at least 10 temperate exoplanets in a feasible and affordable manner [Voyage 2050 Senior Committee, 2021].

So, what has changed such that a MIR space interferometer may be seen as feasible once again? Admittedly, the *Darwin* and TPF-I missions were rather premature, especially considering the state of exoplanet research in the 2000s (where there were less than 500 planets known, and fewer than 10 planets with a known radius less than three Earth radii) [NASA Exoplanet Science Institute, 2023]. At the time, there was no confidence that a multi billion dollar mission such as TPF-I or *Darwin* would even find terrestrial planets. Everything changed with the *Kepler* observatory [Borucki et al., 2010], where we can now confidently estimate that most stellar systems have planets around them [Cassan et al., 2012], and specifically about 50% of solar-type stars have a terrestrial sized planet in the habitable zone [Bryson et al., 2021]. Multiple planet population studies have shown that a mission like LIFE, targeting stars less than 20 pc away, should be able to detect between 25 and 45 terrestrial planets in the HZ of their host star, though with most of them being found around M-dwarfs [Kammerer & Quanz, 2018; Quanz et al., 2022].

While space interferometry may have stalled for a decade or so, that did not mean that nulling interferometry was not still pursued, albeit in a limited way compared to the *Darwin*/TPF-I mission studies. The first operational, separated aperture nulling interferometer was installed on the Keck telescopes, known as the Keck Interferometer [Colavita et al., 2013], including a nulling mode [Serabyn et al., 2012] with the purpose of both developing the technology for TPF-I, as well as examining the exozodiacal dust emission for nearby stars [Millan-Gabet et al., 2011; Mennesson et al., 2014]. Unfortunately, the Keck Interferometer was discontinued in 2012. Despite this, nulling interferometry is still pursued on the Keck telescopes, particularly in the form of Vortex Fibre Nulling [Echeverri et al., 2019], albeit with only a single aperture. Single aperture nulling was also investigated through the Palomar Fibre Nuller (PFN) project [Serabyn et al., 2019], which aimed to demonstrate the detection capabilities of a rotating baseline interferometer and also produced the "Null Self Calibration" technique of statistically calibrating the null depth between two apertures [e.g. Hanot et al., 2011; Mennesson et al., 2011]. Finally, the previously mentioned BLINC instrument [Hinz et al., 2000] was used as a precursor to a larger nulling interferometer attached to the Large Binocular Telescope (i.e. the LBTI; [Hinz et al., 2003, 2014, 2016; Defrère et al., 2016]), which has been very successful in continuing the measurement of exozodiacal dust through the HOSTS [Ertel et al., 2020] survey and is still in use today.

Major technological improvements have also been made in the past decade or so. Integrated optic (IO) beam combiners, essentially the equivalent of an electronic circuit but using light in a glass substrate, have shown promise in demonstrating nulling at NIR wavelengths on a much smaller platform compared to classical bulk optic combiners, while also exhibiting spatial filtering properties [e.g. Martin et al., 2017; Sanny et al., 2022]. One particularly fruitful research group is the GLINT (Guided-Light Interferometric Nulling Technology) team, who have demonstrated IO nulling beam combiners for aperture masking interferometry [Norris et al., 2020; Lagadec et al., 2021], including using photonic tricouplers for achromatic nulling [Martinod et al., 2021; Klinner-Teo et al., 2022]. A photonic tricoupler has also been shown to be useful for classical beam combination and visibility recovery, rather than nulling [Hansen et al., 2022].

Perhaps most critically, formation flight at the centimetre level has been demonstrated with the PRISMA mission [D'Amico et al., 2012], and the near-future PROBA-3 mission will hopefully demonstrate even more precise sub-millimetre position accuracy [Focardi et al., 2015]. Such demonstrations are critical, as numerous studies have shown that fringe tracking OPD residuals need to be at the 1 nm level for sufficient stellar nulling [e.g. Lay, 2004; Dannert et al., 2022], and while much of this positioning can be done with a piezo-electric stage delay line, the spacecraft must stay within the stroke range of this stage (nominally a few mm to 1 cm). As explored by Monnier et al. [2019], numerous other satellite missions from outside the astronomy community, in particular the huge increase in small satellite missions, have also investigated formation flight for satellite swarms for purposes such as telecommunications and remote sensing. Hence, most of the formation flight architecture has likely been developed and tested in space, albeit not together for the purposes of interferometry.

Another development has been the notion of kernel-nulling, a beam combination and data reduction technique modelled after the concepts of closure phase and its generalisation, kernel phase [Martinache, 2010]. Proposed by Martinache & Ireland [2018], kernel-nulling is based around the ideas of kernels, which are linear combinations of nulling interferometer outputs that are resistant to second order phase errors. In fact, as shown by Laugier et al. [2020], phase chopping is in fact one specific formulation of kernel-nulling.

This technique opens up new avenues of multi-telescope beam combination, and the ability to leverage more information contained in the modulation maps.

However, despite the advances, there are still critical technology gaps and challenges that need to be addressed to ensure a mission like LIFE receives political support and is successful in its mission. First are the challenges associated with formation flight; in particular formation flying interferometry. Despite all the progress mentioned above, we have not yet demonstrated a free-flying interferometer in space with sufficient fringe tracking residuals so as to accomplish the goals of a nulling interferometer. This involves launching a small scale mission to demonstrate fringe tracking with 1 nm residuals, and by extension full 6-dimensional formation flight at the 1 mm level along the optical axis. Other technology gaps include sufficient injection into a single-mode fibre and pupil stabilisation in a formation flying environment. Such small satellite mission concepts are being studied, such as by Dandumont et al. [2020], Matsuo et al. [2022] and Hansen & Ireland [2020]. This latter mission is the planned successor to a ground-based formation flying testbed interferometer named *Pyxis*, which aims to demonstrate the metrology and positioning accuracy required for such a space mission. The development and testing of *Pyxis* is explored in Hansen et al. [2022]; Hansen et al. [2023b].

The other major challenges are associated with the nulling aspect of the LIFE mission. These include obtaining a sufficiently deep and broad achromatic null over a MIR bandpass in cryogenic conditions, a goal of the Nulling Interferometer Cryogenic Experiment [Ranganathan et al., 2022]. This experiment aims to demonstrate nulling at a minimum of 1×10^{-5} contrast at 40 K, and ideally pushing this contrast down to that obtained by Martin et al. [2012] at 1×10^{-6}. Spatial filtering in the MIR regime is another challenge, due to the fact that silicon based glasses are opaque at those wavelengths, and hence fibres or IO are not feasible in this regime. There are ongoing activities researching chalcogenide glasses and photonic crystal fibres that may work for MIR photonics [e.g. Zhang et al., 2015; Vigreux et al., 2015; Kenchington Goldsmith et al., 2017a,b; Trolès & Brilland, 2017; Butcher et al., 2018; Gretzinger et al., 2019], as well as investigations into the InGaAs/InP optical platform [e.g. Gilles et al., 2015], but substantial progress needs to be made to ensure adequate throughput and waveguide properties.

Finally, with the advent of IO beam combiners and the development of kernel-nulling, there is incentive to revisit the beam combining architectures and telescope configurations used in the *Darwin*/TPF-I era. Such renewed trade studies and architecture investigations, especially including the technique of kernel-nulling and its extension to the LIFE mission are explored thoroughly in Hansen et al. [2022, 2023a].

Bibliography

Absil, O. 2006, PhD thesis, University of Liege, Belgium

Ahrens, T. J. 1995, Global earth physics: a handbook of physical constants, Vol. 1 (American Geophysical Union)

Alei, E., Konrad, B. S., Angerhausen, D., et al. 2022, A&A, 665, A106, doi: 10.1051/0004-6361/202243760

Angel, J. R. P., & Woolf, N. J. 1997, ApJ, 475, 373, doi: 10.1086/303529

Arnold, L., Gillet, S., Lardière, O., Riaud, P., & Schneider, J. 2002, A&A, 392, 231, doi: 10.1051/0004-6361:20020933

Babcock, H. W. 1953, PASP, 65, 229, doi: 10.1086/126606

Baldwin, J. E., Haniff, C. A., Mackay, C. D., & Warner, P. J. 1986, Nature, 320, 595, doi: 10.1038/320595a0

Ballard, S., Fabrycky, D., Fressin, F., et al. 2011, ApJ, 743, 200, doi: 10.1088/0004-637X/743/2/200

Barclay, T., Kostov, V. B., Colón, K. D., et al. 2021, AJ, 162, 300, doi: 10.3847/1538-3881/ac2824

Barnes, J. W., Turtle, E. P., Trainer, M. G., et al. 2021, Planetary Science Journal, 2, 130, doi: 10.3847/PSJ/abfdcf

Battrick, B., ed. 1995, ESA Special Publication, Vol. 1180, Horizon 2000 plus : European space science in the 21st century

Beichman, C., Mennesson, B., Quanz, S., et al. 2023, Towards Other Earths - Exoplanet science with a space-based mid-infrared nulling interferometer: a consensus report from the KISS workshop “Exploring Exoplanets with Interferometry”

Beichman, C. A., Woolf, N. J., & Lindensmith, C. A. 1999, The Terrestrial Planet Finder (TPF) : a NASA Origins Program to search for habitable planets, Tech. rep., Jet Propulsion Laboratory, California Institute of Technology, Pasadena, California

Belikov, R., Bryson, S., Sirbu, D., et al. 2018, in Proc. SPIE, Vol. 10698, Space Telescopes and Instrumentation 2018: Optical, Infrared, and Millimeter Wave, ed. M. Lystrup, H. A. MacEwen, G. G. Fazio, N. Batalha, N. Siegler, & E. C. Tong, 106981H

Belikov, R., Pluzhnik, E., Connelley, M. S., et al. 2010, in Proc. SPIE, Vol. 7731, Space Telescopes and Instrumentation 2010: Optical, Infrared, and Millimeter Wave, ed. J. Oschmann, Jacobus M., M. C. Clampin, & H. A. MacEwen, 77312D

Belikov, R., Sirbu, D., Jewell, J. B., Guyon, O., & Stark, C. C. 2021, in Proc. SPIE, Vol. 11823, Techniques and Instrumentation for Detection of Exoplanets X, ed. S. B. Shaklan & G. J. Ruane, 118230W

Beuzit, J. L., Vigan, A., Mouillet, D., et al. 2019, A&A, 631, A155, doi: 10.1051/0004-6361/201935251

Blackwood, G. H., Lay, O. P., Deininger, W. D., et al. 2003, in Proc. SPIE, Vol. 4852, Interferometry in Space, ed. M. Shao, 463–480

Boccaletti, A., Lagage, P. O., Baudoz, P., et al. 2015, PASP, 127, 633, doi: 10.1086/682256

Boccaletti, A., Cossou, C., Baudoz, P., et al. 2022, A&A, 667, A165, doi: 10.1051/0004-6361/202244578

Boden, A. F. 2000, in Principles of Long Baseline Stellar Interferometry, ed. P. R. Lawson, 9

Bond, I. A., Udalski, A., Jaroszyński, M., et al. 2004, ApJ, 606, L155, doi: 10.1086/420928

Born, M., & Wolf, E. 1999, Principles of Optics (Cambridge University Press)

Borucki, W. J., Koch, D., Basri, G., et al. 2010, Science, 327, 977, doi: 10.1126/science.1185402

Boyajian, T. S., von Braun, K., van Belle, G., et al. 2012, ApJ, 757, 112, doi: 10.1088/0004-637X/757/2/112

Bracewell, R. N. 1978, Nature, 274, 780, doi: 10.1038/274780a0

Bracewell, R. N., & MacPhie, R. H. 1979, Icarus, 38, 136, doi: 10.1016/0019-1035(79)90093-9

Brown, R. H. 1968, ARA&A, 6, 13, doi: 10.1146/annurev.aa.06.090168.000305

Brugger, B., Mousis, O., Deleuil, M., & Lunine, J. I. 2016, ApJ, 831, L16, doi: 10.3847/2041-8205/831/2/L16

Bryson, S., Kunimoto, M., Kopparapu, R. K., et al. 2021, AJ, 161, 36, doi: 10.3847/1538-3881/abc418

Buscher, D. F., & Longair, M. 2015a, Practical Optical Interferometry (Cambridge University Press)

—. 2015b, Interferometers in practice, Cambridge Observing Handbooks for Research Astronomers (Cambridge University Press), 91128

—. 2015c, Making fringes, Cambridge Observing Handbooks for Research Astronomers (Cambridge University Press), 135

—. 2015d, Atmospheric seeing and its amelioration, Cambridge Observing Handbooks for Research Astronomers (Cambridge University Press), 5390

—. 2015e, Interferometric observation of faint objects, Cambridge Observing Handbooks for Research Astronomers (Cambridge University Press), 152179

Butcher, H. L., MacLachlan, D. G., Lee, D., Thomson, R. R., & Weidmann, D. 2018, Optics Express, 26, 10930, doi: 10.1364/OE.26.010930

Carlomagno, B., Delacroix, C., Absil, O., et al. 2020, JATIS, 6, 035005, doi: 10.1117/1.JATIS.6.3.035005

Carrión-González, Ó., García Muñoz, A., Cabrera, J., et al. 2020, A&A, 640, A136, doi: 10.1051/0004-6361/202038101

Carrión-González, Ó., Kammerer, J., Angerhausen, D., et al. 2023, A&A, in press, doi: 10.1051/0004-6361/202347027

Cassan, A., Kubas, D., Beaulieu, J. P., et al. 2012, Nature, 481, 167, doi: 10.1038/nature10684

Catling, D. C., Krissansen-Totton, J., Kiang, N. Y., et al. 2018, Astrobiology, 18, 709, doi: 10.1089/ast.2017.1737

Charbonneau, D., Brown, T. M., Latham, D. W., & Mayor, M. 2000, ApJ, 529, L45, doi: 10.1086/312457

Chauvin, G., Lagrange, A. M., Dumas, C., et al. 2004, A&A, 425, L29, doi: 10.1051/0004-6361:200400056

Cockell, C. S., Herbst, T., Léger, A., et al. 2009, Experimental Astronomy, 23, 435, doi: 10.1007/s10686-008-9121-x

Colavita, M. M., Wizinowich, P. L., Akeson, R. L., et al. 2013, PASP, 125, 1226, doi: 10.1086/673475

Coudé du Foresto, V., Perrin, G., Ruilier, C., et al. 1998, in Proc. SPIE, Vol. 3350, Astronomical Interferometry, ed. R. D. Reasenberg, 856–863

Coudé du Foresto, V., Ridgeway, S., & Mariotti, J.-M. 1997, Astronomy and Astrophysics Supplement Series, 121, 379, doi: 10.1051/aas:1997290

Curiel, S., Ortiz-León, G. N., Mioduszewski, A. J., & Sanchez-Bermudez, J. 2022, AJ, 164, 93, doi: 10.3847/1538-3881/ac7c66

D'Amico, S., Ardaens, J. S., & Larsson, R. 2012, Journal of Guidance, Control and Dynamics, 35, 834, doi: 10.2514/1.55638

Dandumont, C., Defrère, D., Kammerer, J., et al. 2020, JATIS, 6, 035004, doi: 10.1117/1.JATIS.6.3.035004

Dannert, F. A., Ottiger, M., Quanz, S. P., et al. 2022, A&A, 664, A22, doi: 10.1051/0004-6361/202141958

Defrère, D., Absil, O., den Hartog, R., Hanot, C., & Stark, C. 2010, A&A, 509, A9, doi: 10.1051/0004-6361/200912973

Defrère, D., Hinz, P. M., Mennesson, B., et al. 2016, ApJ, 824, 66, doi: 10.3847/0004-637X/824/2/66

Defrère, D., Absil, O., Berger, J. P., et al. 2018a, Experimental Astronomy, 46, 475, doi: 10.1007/s10686-018-9593-2

Defrère, D., Léger, A., Absil, O., et al. 2018b, Experimental Astronomy, 46, 543, doi: 10.1007/s10686-018-9613-2

Del Genio, A. D., Kiang, N. Y., Way, M. J., et al. 2019, ApJ, 884, 75, doi: 10.3847/1538-4357/ab3be8

Des Marais, D. J., Harwit, M. O., Jucks, K. W., et al. 2002, Astrobiology, 2, 153, doi: 10.1089/15311070260192246

Dole, S. H. 1964, Habitable planets for man (Blaisdell Publishing Company)

Echeverri, D., Ruane, G., Jovanovic, N., et al. 2019, in Proc. SPIE, Vol. 11117, Techniques and Instrumentation for Detection of Exoplanets IX, ed. S. B. Shaklan, 111170V

Eisenhauer, F., Monnier, J. D., & Pfuhl, O. 2023, ARA&A, 61, doi: 10.1146/annurev-astro-121622-045019

Ertel, S., Defrère, D., Hinz, P., et al. 2020, AJ, 159, 177, doi: 10.3847/1538-3881/ab7817

Ertel, S., Wagner, K., Leisenring, J., et al. 2022, in Proc. SPIE, Vol. 12183, Optical and Infrared Interferometry and Imaging VIII, ed. A. Mérand, S. Sallum, & J. Sanchez-Bermudez, 1218302

Fizeau, H. 1868, Comptes Rendus Hebdomadaires des Seances de l'Academie des Sciences, 66, 932

Focardi, M., Bemporad, A., Buckley, S., et al. 2015, in Proc. SPIE, Vol. 9604, Solar Physics and Space Weather Instrumentation VI, ed. S. Fineschi & J. Fennelly, 96040D

Foo, G., Palacios, D. M., & Swartzlander, Grover A., J. 2005, Optics Letters, 30, 3308, doi: 10.1364/OL.30.003308

Fridlund, C. V. M. 2002, Planet. Space Sci., 50, 101, doi: 10.1016/S0032-0633(01)00056-3

Fried, D. L. 1966, Journal of the Optical Society of America (1917-1983), 56, 1372

Gaia Collaboration, Prusti, T., de Bruijne, J. H. J., et al. 2016, A&A, 595, A1, doi: 10.1051/0004-6361/201629272

Galicher, R., & Mazoyer, J. 2023, Comptes Rendus. Physique, doi: 10.5802/crphys.133

Gardner, T., Monnier, J. D., Fekel, F. C., et al. 2021, AJ, 161, 40, doi: 10.3847/1538-3881/abcf4e

Gaudi, B. S. 2010, in Exoplanets, ed. S. Seager (The University of Arizona Press), 79–110

—. 2012, ARA&A, 50, 411, doi: 10.1146/annurev-astro-081811-125518

Gaudi, B. S., Seager, S., Mennesson, B., et al. 2019, The Habitable Exoplanet Observatory (HabEx) Mission Concept Study Final Report (Jet Propulsion Laboratory). https://www.jpl.nasa.gov/habex/pdf/HabEx-Final-Report-Public-Release.pdf

Gilles, C., Orbe, L. J., Carpintero, G., Maisons, G., & Carras, M. 2015, Optics Express, 23, 20288, doi: 10.1364/OE.23.020288

Girard, J. H., Leisenring, J., Kammerer, J., et al. 2022, in Proc. SPIE, Vol. 12180, Space Telescopes and Instrumentation 2022: Optical, Infrared, and Millimeter Wave, ed. L. E. Coyle, S. Matsuura, & M. D. Perrin, 121803Q

Glasse, A., Rieke, G. H., Bauwens, E., et al. 2015, PASP, 127, 686, doi: 10.1086/682259

Glindemann, A. 2011, Principles of Stellar Interferometry (Springer), doi: 10.1007/978-3-642-15028-9

Grady, C. A., Proffitt, C. R., Malumuth, E., et al. 2003, PASP, 115, 1036, doi: 10.1086/377083

Gretzinger, T., Gross, S., Arriola, A., & Withford, M. J. 2019, Optics Express, 27, 8626, doi: 10.1364/OE.27.008626

Guyon, O., Mennesson, B., Serabyn, E., & Martin, S. 2013, PASP, 125, 951, doi: 10.1086/671816

Guyon, O., Pluzhnik, E. A., Kuchner, M. J., Collins, B., & Ridgway, S. T. 2006, ApJS, 167, 81, doi: 10.1086/507630

Hand, K. P., Phillips, C. B., Murray, A., et al. 2022, Planetary Science Journal, 3, 22, doi: 10.3847/PSJ/ac4493

Haniff, C. 2007, New Astronomy Reviews, 51, 565, doi: 10.1016/j.newar.2007.06.002

Hanot, C., Mennesson, B., Martin, S., et al. 2011, ApJ, 729, 110, doi: 10.1088/0004-637X/729/2/110

Hansen, J. 2019, Honours thesis, Australian National University

Hansen, J. T., & Ireland, M. J. 2020, PASA, 37, e019, doi: 10.1017/pasa.2020.13

Hansen, J. T., Ireland, M. J., Laugier, R., & LIFE Collaboration. 2023a, A&A, 670, A57, doi: 10.1051/0004-6361/202243863

Hansen, J. T., Ireland, M. J., & LIFE Collaboration. 2022, A&A, 664, A52, doi: 10.1051/0004-6361/202243107

Hansen, J. T., Ireland, M. J., Ross-Adams, A., et al. 2022, JATIS, 8, 025002, doi: 10.1117/1.JATIS.8.2.025002

Hansen, J. T., Wade, S., Ireland, M. J., et al. 2023b, Journal of Astronomical Telescopes, Instruments, and Systems, 9, 045001, doi: 10.1117/1.JATIS.9.4.045001

Hardy, J. W. 1998, Adaptive Optics for Astronomical Telescopes (Oxford University Press)

Hastie, M., & McLeod, B. 2008, in Proc. SPIE, Vol. 7014, Ground-based and Airborne Instrumentation for Astronomy II, ed. I. S. McLean & M. M. Casali, 70140B

Henry, G. W., Marcy, G. W., Butler, R. P., & Vogt, S. S. 2000, ApJ, 529, L41, doi: 10.1086/312458

Hinkley, S., Lacour, S., Marleau, G. D., et al. 2023, A&A, 671, L5, doi: 10.1051/0004-6361/202244727

Hinz, P., Bailey, V. P., Defrère, D., et al. 2014, in Proc. SPIE, Vol. 9146, Optical and Infrared Interferometry IV, ed. J. K. Rajagopal, M. J. Creech-Eakman, & F. Malbet, 91460T

Hinz, P. M., Angel, J. R. P., McCarthy, Donald W., J., Hoffman, W. F., & Peng, C. Y. 2003, in Proc. SPIE, Vol. 4838, Interferometry for Optical Astronomy II, ed. W. A. Traub, 108–112

Hinz, P. M., Angel, J. R. P., Woolf, N. J., Hoffmann, W. F., & McCarthy, D. W. 2000, in Proc. SPIE, Vol. 4006, Interferometry in Optical Astronomy, ed. P. Léna & A. Quirrenbach, 349–353

Hinz, P. M., Defrère, D., Skemer, A., et al. 2016, in Proc. SPIE, Vol. 9907, Optical and Infrared Interferometry and Imaging V, ed. F. Malbet, M. J. Creech-Eakman, & P. G. Tuthill, 990704

Huang, S.-S. 1959, American Scientist, 47, 397

Ireland, M. J., Mérand, A., ten Brummelaar, T. A., et al. 2008, in Proc. SPIE, Vol. 7013, Optical and Infrared Interferometry, ed. M. Schöller, W. C. Danchi, & F. Delplancke, 701324

Jennison, R. C. 1958, MNRAS, 118, 276, doi: 10.1093/mnras/118.3.276

Jovanovic, N., Martinache, F., Guyon, O., et al. 2015, PASP, 127, 890, doi: 10.1086/682989

JWST Transiting Exoplanet Community Early Release Science Team, Ahrer, E.-M., Alderson, L., et al. 2023, Nature, 614, 649, doi: 10.1038/s41586-022-05269-w

Kaltenegger, L., & Fridlund, M. 2005, Advances in Space Research, 36, 1114, doi: 10.1016/j.asr.2005.05.061

Kammerer, J., & Quanz, S. P. 2018, A&A, 609, A4, doi: 10.1051/0004-6361/201731254

Karlsson, A., d'Arcio, L., den Hartog, R., & Fridlund, M. 2006, in Proc. SPIE, Vol. 6265, Space Telescopes and Instrumentation I: Optical, Infrared, and Millimeter, ed. J. C. Mather, H. A. MacEwen, & M. W. M. de Graauw, 62651O

Kasdin, N. J., Bailey, V. P., Mennesson, B., et al. 2020, in Proc. SPIE, Vol. 11443, Space Telescopes and Instrumentation 2020: Optical, Infrared, and Millimeter Wave, ed. M. Lystrup & M. D. Perrin, 114431U

Kasting, J. F., Whitmire, D. P., & Reynolds, R. T. 1993, Icarus, 101, 108, doi: 10.1006/icar.1993.1010

Kenchington Goldsmith, H.-D., Cvetojevic, N., Ireland, M., & Madden, S. 2017a, Optics Express, 25, 3038, doi: 10.1364/OE.25.003038

Kenchington Goldsmith, H.-D., Ireland, M., Ma, P., Cevetojevic, N., & Madden, S. 2017b, Optics Express, 25, 16813, doi: 10.1364/OE.25.016813

Kitzmann, D., Patzer, A. B. C., von Paris, P., Godolt, M., & Rauer, H. 2011, A&A, 531, A62, doi: 10.1051/0004-6361/201014343

Klinner-Teo, T., Martinod, M.-A., Tuthill, P., et al. 2022, JATIS, 8, 045001, doi: 10.1117/1.JATIS.8.4.045001

Konacki, M., Torres, G., Jha, S., & Sasselov, D. D. 2003, Nature, 421, 507, doi: 10.1038/nature01379

Konrad, B. S., Alei, E., Quanz, S. P., et al. 2022, A&A, 664, A23, doi: 10.1051/0004-6361/202141964

Kopparapu, R. K., Ramirez, R., Kasting, J. F., et al. 2013, ApJ, 765, 131, doi: 10.1088/0004-637X/765/2/131

Labeyrie, A. 1975, ApJ, 196, L71, doi: 10.1086/181747

Labeyrie, A., Authier, B., de Graauw, T., Kibblewhite, E., & Weigelt, G. 1985, in ESA Special Publication, Vol. 226, Kilometric Optical Arrays in Space, ed. N. Longdon & O. Melita, 27–33

Labeyrie, A., Lipson, S. G., & Nisenson, P. 2014, An Introduction to Optical Stellar Interferometry (Cambridge University Press)

Labeyrie, A., Praderie, F., Steinberg, J., Vatoux, S., & Wouters, F. 1980, in Optical and Infrared Telescopes for the 1990's, ed. A. Hewitt, 1020

Lagadec, T., Norris, B., Gross, S., et al. 2021, PASA, 38, e036, doi: 10.1017/pasa.2021.29

Laugier, R., Cvetojevic, N., & Martinache, F. 2020, A&A, 642, A202, doi: 10.1051/0004-6361/202038866

Laugier, R., Defrère, D., Courtney-Barrer, B., et al. 2023, A&A, 671, A110, doi: 10.1051/0004-6361/202244351

Lawson, P. 2000, Principles of Long Baseline Stellar Interferometry (JPL). https://ecommons.cornell.edu/handle/1813/41240

Lawson, P. R. 2000, in Principles of Long Baseline Stellar Interferometry, ed. P. R. Lawson, 113

Lay, O. P. 2004, Appl. Opt., 43, 6100, doi: 10.1364/AO.43.006100

—. 2005, Appl. Opt., 44, 5859, doi: 10.1364/AO.44.005859

Lay, O. P. 2006, in Proc. SPIE, Vol. 6268, Advances in Stellar Interferometry, ed. J. D. Monnier, M. Schöller, & W. C. Danchi, 62681A

Lay, O. P., Martin, S. R., & Hunyadi, S. L. 2007, in Proc. SPIE, Vol. 6693, Techniques and Instrumentation for Detection of Exoplanets III, ed. D. R. Coulter, 66930A

Lay, O. P., Gunter, S. M., Hamlin, L. A., et al. 2005, in Proc. SPIE, Vol. 5905, Techniques and Instrumentation for Detection of Exoplanets II, ed. D. R. Coulter, 8–20

Le Duigou, J. M., Ollivier, M., Léger, A., et al. 2006, in Proc. SPIE, Vol. 6265, Space Telescopes and Instrumentation I: Optical, Infrared, and Millimeter, ed. J. C. Mather, H. A. MacEwen, & M. W. M. de Graauw, 62651M

Léger, A., Fontecave, M., Labeyrie, A., et al. 2011, Astrobiology, 11, 335, doi: 10.1089/ast.2010.0516

Léger, A., Mariotti, J. M., Mennesson, B., et al. 1996, Icarus, 123, 249, doi: 10.1006/icar.1996.0155

Leinert, C., Bowyer, S., Haikala, L. K., et al. 1998, A&AS, 127, 1, doi: 10.1051/aas:1998105

LIFE Collaboration. 2023, LIFE Space Mission. https://www.life-space-mission.com/

Line, M., Quanz, S. P., Schwieterman, E. W., et al. 2019, BAAS, 51, 271

Lopez, B., Lagarde, S., Petrov, R. G., et al. 2022, A&A, 659, A192, doi: 10.1051/0004-6361/202141785

Lovis, C., & Fischer, D. 2010, in Exoplanets, ed. S. Seager (The University of Arizona Press), 27–53

Macintosh, B., Graham, J. R., Ingraham, P., et al. 2014, Proceedings of the National Academy of Science, 111, 12661, doi: 10.1073/pnas.1304215111

Macintosh, B., Graham, J. R., Barman, T., et al. 2015, Science, 350, 64, doi: 10.1126/science.aac5891

Martin, S., Booth, A., Liewer, K., et al. 2012, Appl. Opt., 51, 3907, doi: 10.1364/AO.51.003907

Martin, S., Ksendzov, A., Lay, O., Peters, R. D., & Scharf, D. P. 2011, in Proc. SPIE, Vol. 8151, Techniques and Instrumentation for Detection of Exoplanets V, ed. S. Shaklan, 81510D

Martin, S., Serabyn, G., Liewer, K., & Mennesson, B. 2017, Optica, 4, 110, doi: 10.1364/OPTICA.4.000110

Martinache, F. 2010, ApJ, 724, 464, doi: 10.1088/0004-637X/724/1/464

Martinache, F., & Ireland, M. J. 2018, A&A, 619, A87, doi: 10.1051/0004-6361/201832847

Martinod, M.-A., Tuthill, P., Gross, S., et al. 2021, Appl. Opt., 60, D100, doi: 10.1364/AO.423541

Mather, J. 2005, Project Status for the CAA. https://web.archive.org/web/20081110180605/http://www7.nationalacademies.org/bpa/CAA_Nov2005_Presentation_Mather.pdf

Matsuo, T., Ikari, S., Kondo, H., et al. 2022, JATIS, 8, 015001, doi: 10.1117/1.JATIS.8.1.015001

Mayor, M., & Queloz, D. 1995, Nature, 378, 355, doi: 10.1038/378355a0

McIntyre, S. R. N., King, P. L., & Mills, F. P. 2023, MNRAS, 519, 6210, doi: 10.1093/mnras/stad095

McKay, D. S., Gibson, Everett K., J., Thomas-Keprta, K. L., et al. 1996, Science, 273, 924, doi: 10.1126/science.273.5277.924

Mennesson, B., Hanot, C., Serabyn, E., et al. 2011, ApJ, 743, 178, doi: 10.1088/0004-637X/743/2/178

Mennesson, B., Léger, A., & Ollivier, M. 2005, Icarus, 178, 570, doi: 10.1016/j.icarus.2005.05.012

Mennesson, B., & Mariotti, J. M. 1997, Icarus, 128, 202, doi: 10.1006/icar.1997.5731

Mennesson, B., Millan-Gabet, R., Serabyn, E., et al. 2014, ApJ, 797, 119, doi: 10.1088/0004-637X/797/2/119

Mennesson, B., Defrère, D., Nowak, M., et al. 2016, in Proc. SPIE, Vol. 9907, Optical and Infrared Interferometry and Imaging V, ed. F. Malbet, M. J. Creech-Eakman, & P. G. Tuthill, 99070X

Michelson, A. A. 1920, Contributions from the Mount Wilson Observatory / Carnegie Institution of Washington, 184, 1

Michelson, A. A., & Pease, F. G. 1921, ApJ, 53, 249, doi: 10.1086/142603

Millan-Gabet, R., Serabyn, E., Mennesson, B., et al. 2011, ApJ, 734, 67, doi: 10.1088/0004-637X/734/1/67

Monnier, J., Aarnio, A., Absil, O., et al. 2019, in BAAS, Vol. 51, 153

Monnier, J. D. 2000, in Principles of Long Baseline Stellar Interferometry, ed. P. R. Lawson, 203

Monnier, J. D. 2001, PASP, 113, 639, doi: 10.1086/320288

Monnier, J. D. 2003, Reports on Progress in Physics, 66, 789, doi: 10.1088/0034-4885/66/5/203

NASA Exoplanet Science Institute. 2023, NASA Exoplanet Archive. https://exoplanetarchive.ipac.caltech.edu/index.html

National Academies of Sciences, Engineering, and Medicine. 2021, Pathways to Discovery in Astronomy and Astrophysics for the 2020s (Washington, DC: The National Academies Press), doi: 10.17226/26141

Noordam, J. E., Atherton, P. D., & Greenaway, A. H. 1985, in ESA Special Publication, Vol. 226, Kilometric Optical Arrays in Space, ed. N. Longdon & O. Melita, 63–69

Norris, B. R. M., Cvetojevic, N., Lagadec, T., et al. 2020, MNRAS, 491, 4180, doi: 10.1093/mnras/stz3277

O'Brien, D. P., Walsh, K. J., Morbidelli, A., Raymond, S. N., & Mandell, A. M. 2014, Icarus, 239, 74, doi: 10.1016/j.icarus.2014.05.009

Otárola, A., Richter, M., Packham, C., & Chun, M. 2015, in Journal of Physics Conference Series, Vol. 595, Journal of Physics Conference Series, 012023

Perryman, M., Hartman, J., Bakos, G. Á., & Lindegren, L. 2014, ApJ, 797, 14, doi: 10.1088/0004-637X/797/1/14

Peters, R. D., Lay, O. P., & Lawson, P. R. 2010, PASP, 122, 85, doi: 10.1086/649850

Petrov, R. G., Malbet, F., Weigelt, G., et al. 2007, A&A, 464, 1, doi: 10.1051/0004-6361:20066496

Price, D. C., Enriquez, J. E., Brzycki, B., et al. 2020, AJ, 159, 86, doi: 10.3847/1538-3881/ab65f1

Qian, S. B., Liao, W. P., Zhu, L. Y., & Dai, Z. B. 2010, ApJ, 708, L66, doi: 10.1088/2041-8205/708/1/L66

Quanz, S. P., Absil, O., Benz, W., et al. 2021, Experimental Astronomy, doi: 10.1007/s10686-021-09791-z

Quanz, S. P., Ottiger, M., Fontanet, E., et al. 2022, A&A, 664, A21, doi: 10.1051/0004-6361/202140366

Quirrenbach, A. 2010, in Exoplanets, ed. S. Seager (The University of Arizona Press), 157–174

Rackham, B. V., Apai, D., & Giampapa, M. S. 2018, ApJ, 853, 122, doi: 10.3847/1538-4357/aaa08c

Rains, A. D., Ireland, M. J., White, T. R., Casagrande, L., & Karovicova, I. 2020, MNRAS, 493, 2377, doi: 10.1093/mnras/staa282

Rains, A. D., Žerjal, M., Ireland, M. J., et al. 2021, MNRAS, 504, 5788, doi: 10.1093/mnras/stab1167

Ranganathan, M., Glauser, A. M., Birbacher, T., Gheorghe, A. A., & Quanz, S. P. 2022, in Proc. SPIE, Vol. 12183, Optical and Infrared Interferometry and Imaging VIII, ed. A. Mérand, S. Sallum, & J. Sanchez-Bermudez, 121830L

Reinhard, C. T., Olson, S. L., Schwieterman, E. W., & Lyons, T. W. 2017, Astrobiology, 17, 287, doi: 10.1089/ast.2016.1598

Roddier, F. 1981, Progess in Optics, 19, 281, doi: 10.1016/S0079-6638(08)70204-X

Rouan, D., Riaud, P., Boccaletti, A., Clénet, Y., & Labeyrie, A. 2000, PASP, 112, 1479, doi: 10.1086/317707

Sagan, C., Thompson, W. R., Carlson, R., Gurnett, D., & Hord, C. 1993, Nature, 365, 715, doi: 10.1038/365715a0

Sanny, A., Gross, S., Labadie, L., et al. 2022, in Proc. SPIE, Vol. 12183, Optical and Infrared Interferometry and Imaging VIII, ed. A. Mérand, S. Sallum, & J. Sanchez-Bermudez, 1218316

Schwieterman, E. W., Kiang, N. Y., Parenteau, M. N., et al. 2018, Astrobiology, 18, 663, doi: 10.1089/ast.2017.1729

Seager, S., Turner, E. L., Schafer, J., & Ford, E. B. 2005, Astrobiology, 5, 372, doi: 10.1089/ast.2005.5.372

Seo, B.-J., Patterson, K., Balasubramanian, K., et al. 2019, in Proc. SPIE, Vol. 11117, Proc. SPIE, 111171V

Serabyn, E., Mennesson, B., Colavita, M. M., Koresko, C., & Kuchner, M. J. 2012, ApJ, 748, 55, doi: 10.1088/0004-637X/748/1/55

Serabyn, E., Mennesson, B., Martin, S., Liewer, K., & Kühn, J. 2019, MNRAS, 489, 1291, doi: 10.1093/mnras/stz2163

Shaklan, S. B., Colavita, M. M., & Shao, M. 1992, in European Southern Observatory Conference and Workshop Proceedings, Vol. 39, European Southern Observatory Conference and Workshop Proceedings, 1271–1283

Silvotti, R., Schuh, S., Janulis, R., et al. 2007, Nature, 449, 189, doi: 10.1038/nature06143

Stachnik, R. V., & Gezari, D. Y. 1985, in ESA Special Publication, Vol. 226, Kilometric Optical Arrays in Space, ed. N. Longdon & O. Melita, 35–42

Stadler, E., Diolaiti, E., Schreiber, L., et al. 2022, in Proc. SPIE, Vol. 12185, Adaptive Optics Systems VIII, ed. L. Schreiber, D. Schmidt, & E. Vernet, 121854E

Stapelfeldt, K. R. 2006, in The Scientific Requirements for Extremely Large Telescopes, ed. P. Whitelock, M. Dennefeld, & B. Leibundgut, Vol. 232, 149–158

Stark, C. C., Roberge, A., Mandell, A., & Robinson, T. D. 2014, ApJ, 795, 122, doi: 10.1088/0004-637X/795/2/122

Steele, A., Beaty, D., Amend, J., et al. 2006, Findings of the Astrobiology Field Lab Science Steering Group (AFLSSG) (Mars Exploration Program Analysis Group)

Taylor, G. I. 1938, Proceedings of the Royal Society of London Series A, 164, 476, doi: 10.1098/rspa.1938.0032

ten Brummelaar, T. A., McAlister, H. A., Ridgway, S. T., et al. 2005, ApJ, 628, 453, doi: 10.1086/430729

The LUVOIR Team. 2019, The LUVOIR Mission Concept Study Final Report (National Aeronautics and Space Administration). https://asd.gsfc.nasa.gov/luvoir/resources/docs/LUVOIR_FinalReport_2019-08-26.pdf

Thiébaut, E., & Mugnier, L. 2006, in IAU Colloq. 200: Direct Imaging of Exoplanets: Science & Techniques, ed. C. Aime & F. Vakili, 547–552

Tinetti, G., & Beaulieu, J.-P. 2009, in Transiting Planets, ed. F. Pont, D. Sasselov, & M. J. Holman, Vol. 253, 231–237

Traub, W. A., & Carleton, N. P. 1985, in ESA Special Publication, Vol. 226, Kilometric Optical Arrays in Space, ed. N. Longdon & O. Melita, 43–48

Trolès, J., & Brilland, L. 2017, Comptes Rendus Physique, 18, 19, doi: 10.1016/j.crhy.2016.09.001

Vago, J. L., Westall, F., Pasteur Instrument Team, et al. 2017, Astrobiology, 17, 471, doi: 10.1089/ast.2016.1533

van Cittert, P. 1934, Physica, 1, 201, doi: 10.1016/S0031-8914(34)90026-4

Vigreux, C., Escalier, R., Pradel, A., et al. 2015, Optical Materials, 49, 218, doi: 10.1016/j.optmat.2015.09.025

Voyage 2050 Senior Committee. 2021, Voyage 2050 - Final Recommendations from the Voyage 2050 Senior Committee (European Space Agency). https://www.cosmos.esa.int/documents/1866264/1866292/Voyage2050-Senior-Committee-report-public.pdf/e2b2631e-5348-5d2d-60c1-437225981b6b?t=1623427287109

Wallner, O., Ergenzinger, K., Flatscher, R., & Johann, U. 2006, in Proc. SPIE, Vol. 6268, Advances in Stellar Interferometry, ed. J. D. Monnier, M. Schöller, & W. C. Danchi, 626827

Walter, A. B., Noyes, M., Meeker, S., et al. 2022, in American Astronomical Society Meeting Abstracts, Vol. 54, American Astronomical Society Meeting Abstracts, 408.06

Williams, D. R. 2022, Mars Fact Sheet. https://nssdc.gsfc.nasa.gov/planetary/factsheet/marsfact.html

—. 2023, Jupiter Fact Sheet. https://nssdc.gsfc.nasa.gov/planetary/factsheet/jupiterfact.html

Winn, J. N. 2010, in Exoplanets, ed. S. Seager (The University of Arizona Press), 55–77

Wolszczan, A., & Frail, D. A. 1992, Nature, 355, 145, doi: 10.1038/355145a0

Wolszczan, A., & Kuchner, M. 2010, in Exoplanets, ed. S. Seager (The University of Arizona Press), 175–190

Wong, I., Shporer, A., Daylan, T., et al. 2020, AJ, 160, 155, doi: 10.3847/1538-3881/ababad

Young, T. 1807, A course of lectures on natural philosophy and the mechanical arts: in two volumes, Vol. 2 (Johnson)

Zernike, F. 1938, Physica, 5, 785, doi: 10.1016/S0031-8914(38)80203-2

Zhang, P., Zhang, J., Yang, P., et al. 2015, Optical Fiber Technology, 26, 176, doi: 10.1016/j.yofte.2015.09.002